Virus-induced vesicular acidification enhances HIV immune evasion.

Marianne E. Yaple-Maresh[1], Giselle G. Flores[2], Gretchen E. Zimmerman[1], Francisco Gomez-Rivera[3], Kathleen L. Collins[1,2,3*]

[1]Department of Internal Medicine, University of Michigan, Ann Arbor, MI, 48109, United States; [2]Graduate Program in Biological Chemistry, [3]Graduate Program in Immunology, University of Michigan, Ann Arbor, MI, 48109, United States

[*]Lead contact: klcollin@med.umich.edu

Gretchen E. Zimmerman was previously affiliated with the Department of Internal Medicine and is currently affiliated with Corewell Health, St. Joseph, MI, United States.

SUMMARY

To inhibit endocytic entry of some viruses, cells promote acidification of endosomes by expressing the short isoform of human nuclear receptor 7 (NCOA7) which increases activity of vacuolar ATPase (V-ATPase). While we found that HIV-1 infection of primary T cells led to acidification of endosomes, NCOA7 levels were only marginally affected. Contrastingly, levels of the 50 kDa form of the sodium/hydrogen exchanger 6 (NHE6) were greatly reduced. NHE6 overexpression and low concentrations of the V-ATPase inhibitor, concanamycin A, selectively reversed endosomal acidification. Endosomal neutralization by these interventions also reduced Nef-dependent MHC-I downmodulation by our wildtype HIV reporter virus. NHE6 overexpression disrupted MHC-I downmodulation by reducing recruitment of Nef to $Rab11^{+}$ compartments and inhibiting interactions between Nef, β-COP, and ARF-1. In addition, we found that the HIV Vif protein was required for downmodulation of the 50 kDa form of NHE6 and for endosomal acidification but was dispensable for Nef-dependent MHC-I downmodulation.

KEYWORDS

HIV, Nef, MHC, antigen presentation, virus, innate, immune, acidification, VATPase, beta COP, ARF-1, AP-1, NHE, NCOA7

INTRODUCTION

The pH of secretory compartments plays an important role in host-pathogen interactions. For pathogens such as influenza that enter a cell through endosomes, acidic pH triggers conformational changes that promote viral fusion and entry of the viral capsid into the cytosol[1]. However, enhanced endosomal acidification can also be protective against viral infection. For example, interferon, which is upregulated in response to viral pathogens, induces human nuclear receptor coactivator 7 (NCOA7), which interacts with the proton pump Vacuolar ATPase (V-ATPase) and promotes vesicle acidification to such an extent that it inhibits influenza and severe acute respiratory syndrome (SARS) coronavirus infection[2,3]. Unlike influenza and coronavirus, HIV enters through the cell membrane rather than endosomes and thus its entry is not modulated substantially by changes in pH[4]. It is not known whether expression of NCOA7 and/or other proteins that modulate V-ATPase activity are altered following HIV infection.

In addition to NCOA7 and V-ATPase, endosomal pH is determined in part by members of the sodium/hydrogen exchanger (NHE) family, which fine tune the pH by leaking protons in exchange for sodium ions[5]. NHE family members selectively localize to specific cellular compartments so that compartment-specific pH can be maintained[5]. Overexpression of NHEs can be used as a tool to increase pH in a specific compartment and to identify the location of pH-dependent steps in trafficking pathways[6,7].

While entry of wildtype HIV is unlikely to be inhibited by changes in pH, research utilizing concanamycin A (CMA), a V-ATPase inhibitor that disrupts acidification, indicates there may be pH sensitive steps in HIV immune evasion pathways[8]. HIV-1 evades recognition by anti-HIV cytotoxic T lymphocytes (CTLs) through disruption of antigen presentation by MHC-I. The mechanism depends on the viral protein Nef, which binds to MHC-I and recruits host intracellular trafficking proteins (AP-1, ARF-1 and β-COP) that target Nef-MHC-I complexes into the endolysosomal pathway from the TGN and accelerate transit to lysosomes[9–11]. Recently, we reported that CMA potently inhibits Nef-dependent MHC-I trafficking and sensitizes HIV-infected primary T cells to anti-HIV CTLs [8].

CMA is known to block lysosomal acidification through inhibition of V-ATPase. However, CMA does not impact lysosome acidification at the very low concentrations that inhibit Nef, especially in primary T cells. Thus, we hypothesized that low dose CMA may counteract Nef-dependent MHC-I downmodulation by disrupting a necessary pH-dependent step in pre-lysosomal compartments along the secretory pathway.

Consistent with this, we found that selective neutralization of transferrin$^+$ endosomal compartments by overexpression of sodium/proton exchanger NHE6 was inhibitory to Nef.

Moreover, HIV infection of activated primary T cells resulted in a dramatic downmodulation of the 50 kDa form of NHE6. Further, the HIV-1 accessory protein Vif was responsible for reduced expression of the 50 kDa form of NHE6. Our results indicate that HIV has evolved to take advantage of and promote acidification of endosomal compartments to facilitate recruitment of intracellular trafficking factors and target MHC-I for degradation, evading the anti-HIV immune response.

RESULTS

HIV-1 infection leads to striking reductions in the 50 kDa form of NHE6 expression, and enhanced acidification of intracellular compartments.

As part of an innate immune response to some viral infections, levels of the V-ATPase interacting protein, NCOA7, are increased, which increases V-ATPase activity and lowers the pH of endocytic vesicles[12]. The resulting increase in acidity is inhibitory to influenza and SARS coronavirus entry through this route[2]. Whether other viruses, such as HIV, trigger similar changes is currently unknown. In addition to V-ATPase, endosomal pH is regulated by sodium/hydrogen exchangers (NHEs) that release protons in the opposite direction of V-ATPase. To assess the impact of HIV infection on these proteins, we performed western blot analysis of primary T cells transduced with a VSV-G pseudotyped replication defective HIV construct expressing a GFP marker (Figure 1A, top panel). Because the HIV *nef* gene is a key pathogenic factor that affects intracellular trafficking in virally infected cells, we examined infection plus and minus Nef expression (Nef-negative mutant referred to as ΔGPEN). For these experiments, we separated the infected (GFP+) from the uninfected (GFP-) cell subsets by fluorescence activated flow cytometric sorting (FACS) (Figure 1B and Supplemental Figure S1A) prior to western blot analysis. As shown in Figure 1C and summarized in Figure 1E we observed a significant increase in NCOA7 protein expression in the GFP+ subset of the wildtype virus that was not altered by Nef expression.

Because sodium hydrogen exchangers oppose V-ATPase activity to increase the pH of endosomal compartments, we examined expression of NHE6, 8 and 9, which localize to different intracellular compartments. NHE6 is the sodium/proton exchanger that localizes to the recycling endosome[5,13], NHE8 localizes to the *mid* and *trans*-Golgi[5], and NHE9 localizes to the late endosome[5]. Consistent with published results, NHE8 and 9 migrates as a single species at approximately 75 kDa. In contrast, NHE6 migrates as multiple forms that include high molecular weight oligomers and aggregates as well as smaller, 50 and/or 75 kDa forms that can vary with

the cell type [14–17]. Given the complexity, we confirmed the bands labeled as NHE6 in Figure 1D were bona fide forms of the protein by using the NHE6 peptide epitope to competitively inhibit specific antibody binding (Supplemental Figure S1B and C).

Surprisingly, following exposure to HIV (plus or minus Nef), infected (GFP+) cells had approximately 65-fold less of the 50 kDa form of NHE6 (Figure 1D, and summarized in 1F). In contrast, levels of NHE8 slightly but significantly increased (Figure 1D, summarized in Figure 1G) and NHE9 levels did not significantly change (Figure 1D, and summarized in 1H). Levels of V-ATPase subunit E did not significantly change in response to HIV infection (Figure 1D and summarized in Figure 1I).

The observation that NHE6 expression decreased while NCOA7 levels slightly, but significantly increased upon infection led us to hypothesize that the pH of endosomal compartments may become more acidic upon infection with HIV-1. To test this, we monitored the effect of HIV on the pH of compartments that are occupied by an endosomal marker, transferrin, which is endocytosed and delivered to the recycling endosome (RE) before being trafficked back the cell surface[18]. We first confirmed that transferrin localizes to the RE in a T cell line, CEM-A2[11], by assessing its localization relative to Rab11, a marker of the RE, and NHE6. We found most, but not all, transferrin colocalized with Rab11 and NHE6 under the conditions of our assay (Supplemental Figure S1D). Based on these results, we utilized transferrin conjugated to a pH-sensitive dye (pHrodo Red) to assess the pH of compartments containing NHE6. To control for potential differences in the amount of pHrodo-transferrin taken up by the cells upon infection, we also included transferrin conjugated to AlexaFluor 647 (AF-647), a dye that is not known to have pH-dependent properties. Thus, changes in transferrin$^+$ compartmental pH could be monitored by normalizing the pHrodo-transferrin signal to the AF-647-transferrin signal.

Consistent with our hypothesis, we found that transferrin$^+$ compartments from infected (GFP+) primary T cells were significantly more acidic than uninfected (GFP-) cells in the same culture (Figure 1J). Together, these data suggest the hypothesis that the HIV-1-induced decrease in the 50 kDa form of NHE6 contributed to the decrease in pH of endosomal compartments. Moreover, based on colocalization of transferrin with Rab11 at the time of pH assessment (Supplemental Figure S1D), the impacted compartments included REs.

V-ATPase inhibitors neutralize transferrin$^+$ compartmental pH at concentrations that reverse Nef activity.

Given the changes in NHE6 expression and endosomal pH we observed upon HIV infection, we sought to determine their significance for HIV-mediated disruption of intracellular

trafficking. For example, HIV Nef mediates disruption of MHC-I trafficking to promote immune evasion. Moreover, this activity of Nef appears to be pH-dependent as it is blocked by V-ATPase inhibitors such as concanamycin A (CMA)[8]. As shown in Figure 2A, CMA reversed Nef-dependent MHC-I downmodulation (referred to as Nef activity) at very low concentrations (IC_{50} ~0.1nM) that were well below what is needed to impact lysosomal acidification (IC_{50} ~1nM). In contrast, the CMA IC_{50} for transferrin$^+$ compartmental neutralization was very similar to that for reversal of Nef activity (Figure 2B). Furthermore, both were lower than that required for lysosome neutralization (Figure 2C). Similar results were obtained using another V-ATPase inhibitor, Bafilomycin A1 (Baf A1) that inhibits Nef at higher concentrations than CMA, but still shows a substantial difference between the Nef activity IC_{50} and the IC_{50} for lysosomal neutralization (Figure 2D)[8]. As observed with CMA, we found that the amount of Baf A1 required to neutralize transferrin$^+$ compartments was very similar to that required to inhibit Nef activity (Figure 2E and F). Taken together, these results support the hypothesis that V-ATPase inhibitors work to reverse Nef activity at least in part by neutralizing endosomal pH and thus that endosomal acidification is required for Nef activity in the wildtype HIV reporter virus.

Viral constructs allow simultaneous HIV infection and NHE overexpression.

To further refine the pH sensitive step in Nef-dependent MHC-I downmodulation, we sought to neutralize compartments selectively via overexpression of organelle specific NHEs. Because NHE6, 8, and 9 are reported to selectively localize to REs[5,6,13], Golgi (*mid* and *trans*)[5] and late endosomes[5] respectively, these constructs provide an approach to selectively neutralize individual intracellular compartments and simultaneously measure their impact on Nef activity. Thus, we created HIV-1 constructs that overexpressed NHE6, 8, or 9 from an internal ribosome entry site (IRES, referred to as ΔGPE-IRES-NHE6/8/9). Overexpression of the NHEs following viral transduction was confirmed with fluorescence confocal microscopy (Figure 3A-F, Supplemental Figure S2A and Supplemental Figure S2B for western blot confirmation). In addition, we confirmed that each overexpressed NHE localized as expected relative to organelle markers and that overexpressed NHEs localize with the markers in a manner similar to endogenously expression NHEs (Figure 3G-L and Supplemental Figure S3A-C). Because Nef is known to interact with one of the organelle markers (AP-1), we confirmed that the staining patterns of AP-1 in mock infected cells were similar to those transduced with the Nef expressing viral construct (Supplemental Figure S3B).

Overexpression of endosomal sodium/hydrogen exchangers reduces the ability of HIV-1 Nef to disrupt MHC-I trafficking.

After confirming that the NHE-containing viruses appropriately overexpressed the NHEs and localized to the expected target compartment, we examined the effect of their overexpression on Nef-dependent MHC-I or CD4 downmodulation. We found that overexpression of all the NHEs tested significantly reduced Nef-dependent MHC-I downmodulation (Figure 4A and B). In fact, overexpression of NHE6 and NHE9 reduced MHC-I downmodulation to similar levels observed with a Nef negative mutant (ΔGPEN). Overexpression of NHEs also inhibited Nef-dependent CD4 downmodulation but was only significant for NHE6 and CD4 downmodulation remained higher than for cells transduced with the Nef negative mutant virus (Figure 4C). Thus, the impact of NHE overexpression overall appears greater for MHC-I than for CD4.

To determine whether the overexpression we achieved with NHE6 was sufficient to neutralize endosomal compartments, we again utilized transferrin conjugated to pHrodo. Relative to control cells transduced with the "empty" HIV IRES-containing construct, overexpression of NHE6 significantly decreased transferrin$^+$ compartmental acidification (Figure 4D), partially reversing HIV-induced endosomal acidification. In contrast, overexpression of NHE8 and 9 did not significantly counteract HIV-induced endosomal acidification (Figure 3E), which is consistent with their localization to other compartments. Interestingly, we did not note significant neutralization of transferrin$^+$ compartments or change in surface MHC-I expression from NHE6 overexpression in the absence of HIV infection (Supplemental Figure S4A and B). Importantly, overexpression of the NHEs did not neutralize lysosomal pH in primary T cells (Figure 4F). In fact, we noted very slight, but significant acidification of the lysosome in response to NHE8 overexpression and infection with ΔGPEN. Taken together, these data support our hypothesis that NHE6 selectively counteracts virus-induced acidification of endosomal compartments which is needed for optimal downmodulation of MHC-I by Nef.

Neutralization of transferrin$^+$ compartments via NHE6 overexpression prevents Nef from binding to cellular proteins required for Nef-mediated disruption of MHC-I trafficking.

Prior studies have reported a requirement for Nef in the *trans*-Golgi where it forms a three-way complex with the MHC-I cytoplasmic tail, and clathrin adaptor protein, AP-1[9,11] in a process that requires the GTPase, ARF-1[9,19]. These interactions are important for Nef to disrupt MHC-I trafficking from the Golgi to the cell surface. Instead, Nef-bound MHC-I traffics to compartments that have not been well characterized where interactions with β-COP of the coatomer complex commit MHC-I to lysosomal degradation[11].

To explore whether compartments containing NHE6 are important for Nef interactions with host trafficking proteins, we constructed a version of the NHE6 overexpressing HIV construct that contained Nef tagged with a FLAG epitope and verified that the insertion of the tag in the N-terminal loop did not affect its ability to downmodulate MHC-I (Figure 5A and B). We observed robust ~50-fold downmodulation of CD4 by FLAG-tagged Nef that was nevertheless slightly less than for wildtype (Figure 5A and B). Western blot analysis of CEM-A2 cell lysates transduced with the "empty vector" version of the IRES construct or NHE6 overexpressing virus before incubation with FLAG beads (input) confirmed expression of proteins of interest (Figure 5C). In addition, we found that the tagged Nef expressed in the empty vector interacted as expected with β-COP, AP-1, MHC-I, and ARF-1 (Figure 5D). Remarkably, we also observed preferential loss of β-COP and ARF-1 with relative preservation of Nef-AP-1 and Nef-MHC-I interactions when NHE6 was overexpressed (Figure 5E). Importantly, we did not observe significant changes in β-COP or ARF-1 expression in response to overexpression of NHE6 (Supplemental Figure S4 C-E). In sum, these data support the conclusion that interactions amongst β-COP, ARF-1 and Nef occur in organelles affected by NHE6 overexpression. Thus, these protein-protein interactions may require an endosome/RE-dependent step and are likely to be pH sensitive. Because both MHC-I and CD4 downmodulation require interactions between Nef and β-COP, these findings provide an explanation for the inhibition of MHC-I and CD4 downmodulation we observed with NHE6 overexpression.

NHE6 overexpression disrupts recruitment of Nef to the recycling endosome.

To further explore a potential pH-sensitive step that requires $Rab11^+$ endosomes/REs, we asked whether Nef localized to $Rab11^+$ compartments in a pH-dependent manner. To accomplish this, we utilized a $CD4^+$ T cell line that stably expressed FLAG-tagged Rab11 (CEM-A2-FLAG-Rab11) and a previously published protocol by which tagged Rab proteins can be used to isolate intact compartments (Figure 6A)[20]. After confirming that these cell lines achieved infection with reporter viruses overexpressing NHE6 (Figure 6B) and confirming our proteins of interest were expressed in whole cell lysates (Figure 2C), we used these cells to isolate $Rab11^+$ vesicles and assessed their protein composition via western blot analysis (Figure 6D). As expected, we detected endogenous and overexpressed NHE6, confirming its natural localization to $Rab11^+$ compartments (Figure 6D). In contrast and as expected, we did not observe NHE8, NHE9, or GAPDH in these purified $Rab11^+$ vesicles. Excitingly, we found that Nef occupies this compartment in infected T cells (Figure 6D). In addition, we found that there was significantly less Nef recruited to $Rab11^+$ compartments upon NHE6 overexpression (Figure 6D and

summarized in 6E). These results provide an explanation for the diminished complex formation we observed with endosomal neutralization by NHE6 overexpression and highlight the importance of Rab11$^+$ compartments for Nef-dependent trafficking in HIV infected cells.

The HIV-1 accessory protein Vif downmodulates the 50 kDa form of NHE6 and contributes to acidification of transferrin$^+$ compartments

Finally, we sought to determine the mechanism by which HIV infection downmodulates the 50 kDa form of NHE6. One possibility is that downmodulation occurs by the action of an HIV factor. To test this hypothesis, we systematically tested the requirement for most of the HIV genes expressed by the reporter construct (*nef, vpr, vif, vpu and tat*) as well as proteins present on the viral particle (VSV-G). As shown in Figure 1D, Nef was not responsible for this phenotype, as the 50 kDa form was downmodulated in cells infected with a virus lacking an intact *nef* gene (ΔGPEN). In addition, the 50 kDa form was still downmodulated in reporter viruses lacking *vpr* and *vpu* (Supplemental Figure S5A and B). Similarly, transduction of cells with virus pseudotyped with a native HIV-1 envelope instead of VSV-G downmodulated the 50 kDa NHE6 form (Supplemental Figure S5C). Moreover, expression of Tat in a lentiviral vector did not lead to changes in expression of NHE6 (Supplemental Figure S5D). In contrast, transduction of cells with a lentiviral construct that overexpressed Vif alone (pscALPS-Vif, Supplemental Figure S5D) was sufficient to decrease expression of the 50 kDa form of NHE6 (Figure 7A). Correspondingly, the 50 kDa form was not downmodulated in cells transduced with the HIV reporter lacking *vif* (ΔGPEF, Figure 7B). Thus, we unexpectedly determined that Vif is the HIV factor that targets NHE6.

To determine whether Vif-mediated downmodulation of the 50 kDa form of NHE6 is responsible for HIV-induced endosomal acidification, we assessed the pH of transferrin$^+$ compartments utilizing transferrin conjugated to pHrodo as described above. Indeed, we found that lack of Vif, but not Nef, counteracted HIV-induced acidification of transferrin$^+$ compartments in primary T cells (Figure 7C).

We then asked whether knock out of *vif* and disruption of HIV-induced endosomal acidification was sufficient to affect Nef-induced MHC-I downmodulation. Surprisingly, we found no statistically significant change in MHC-I downmodulation by Nef in response to knocking out *vif* (Figure 7D). Taken together, our results clearly indicate that Vif is responsible for downmodulation of the 50 kDa form of NHE6 and this correlates to neutralization of transferrin$^+$ compartments as expected. However, neutralization of transferrin$^+$ compartments via *vif* knock out did not impact Nef-dependent MHC-I downmodulation by the Vif-mutant virus. This surprising

result indicates a complex interplay between HIV-1 induced acidification of endosomal compartments, MHC-I trafficking by Nef and targeting of NHE6 expression by HIV through Vif.

DISCUSSION

HIV induced endosomal acidification. Here we describe a link between HIV-1 induced acidification of endosomal compartments and trafficking of MHC-I to the lysosome by Nef. We found a stark Vif-dependent downmodulation of the 50 kDa form of NHE6, a sodium/proton exchanger that localizes to Rab11/transferrin$^+$ compartments. This is complemented by an increase in NCOA7 expression, a protein that promotes vesicular acidification by interacting with V-ATPase. Correspondingly, we observed a significant increase in acidity of transferrin$^+$ compartments during HIV-1 infection that was counteracted by CMA, NHE6 overexpression and disruption of *vif*. Acidification of endosomes has been reported to be protective during some viral infections because it prevents viral entry[12] and promotes antigen presentation via MHC class II[21,22]. While HIV does not enter cells in a manner that is likely to be influenced by increased acidification of endosomal compartments, Nef utilizes these compartments to mis-traffic MHC-I to the lysosome for degradation[23–25].

pH-Dependency of Nef activity. Consistent with a role for endosomal acidification in Nef-dependent MHC-I trafficking, we recently reported the V-ATPase inhibitor CMA blocks Nef-dependent MHC-I downmodulation at concentrations well below those that impact lysosomal pH[26]. Our results showing decreased expression of the 50 kDa form of NHE6 and increase in acidification of transferrin$^+$ compartments led us to hypothesize that CMA may inhibit Nef by disrupting the pH of endosomal compartments occupied by NHE6. In support of this hypothesis, we found that both CMA and Baf A1 neutralized transferrin$^+$ compartmental pH at concentrations similar to those that reversed Nef-dependent MHC-I downmodulation and lower than those that affected the lysosome. These data not only provide novel insight into the mechanism of action of CMA in reversing Nef activity, but also support the hypothesis that wildtype HIV requires hyper-acidification of endosomal compartments for maximal downmodulation of MHC-I.

We further found that selective neutralization of the Golgi network (*mid* and *trans*) and late endosome via overexpression of NHE8, and NHE9 respectively also reduced Nef-dependent MHC-I downmodulation. This is perhaps not surprising as the role of the *trans*-Golgi network and late endosome in mis-trafficking of MHC-I by Nef have been well studied[24,27]. Similarly, it is likely that CMA neutralizes compartments beyond those occupied by transferrin, the focus of our study. While there is a need to further elucidate specific compartments targeted by CMA, our focus on transferrin$^+$ compartments was justified because (i) the role of the *trans*-Golgi network and late

endosome have already been well studied in Nef-dependent MHC-I trafficking while the role of the recycling endosome is not well characterized and (ii) the NHE6 50 kDa form is selectively targeted by HIV.

The role of the Rab11/transferrin$^+$ compartments in Nef-dependent MHC-I trafficking. Excitingly, we found that neutralization of transferrin$^+$ compartments via NHE6 overexpression disrupted complex formation between β-COP, ARF-1, and Nef. While the precise role and identity of these compartments requires further study, these results nevertheless shed light onto an important role for this organelle in Nef-dependent MHC-I trafficking. This conclusion is strengthened by data showing Nef localized to Rab11$^+$ compartments in a pH dependent manner that was disrupted by NHE6 overexpression.

A role for HIV Vif in acidification of endosomal vesicles in HIV infected cells. Studies of knockout or overexpression of HIV-1 accessory proteins revealed the surprising finding that HIV-1 Vif is responsible for downmodulation of the 50 kDa form of NHE6 and corresponding acidification of transferrin$^+$ compartments. Vif has been well-studied as an HIV protein that targets host antiviral factors for proteasomal degradation[28–30] and a similar mechanism may be responsible for the loss of the NHE6 50 kDa form when Vif is expressed.

Unexpectedly we observed no change in Nef-dependent MHC-I downmodulation by the *vif*-mutant virus despite observing significant neuralization of transferrin$^+$ compartments. This interesting finding could suggest that neutralization of transferrin$^+$ compartments via NHE6 overexpression or low dose V-ATPase inhibitor treatment behaves fundamentally different than that of *vif* deletion. Alternatively, the Vif-mutant virus may function differently than wildtype virus for MHC-I downmodulation. Follow up work to investigate this novel role of Vif during HIV-1 infection is required to fully understand this result. From the work presented here, we conclude that during infection with wildtype HIV-1, acidification of endosomal compartments appears to be critical to trafficking of MHC-I to the lysosome by Nef and viral immune evasion.

NHE6 expression is altered during infection of several types of viruses. Prior studies have reported effects of other viral infections on NHE protein expression. Specifically, proteomics analysis of cells infected with Enterovirus 71 revealed that NHE6 expression was significantly diminished[31]. Similarly, a decrease in NHE6 protein expression was observed in the brains of mice infected with Chikungunya virus[32] and a decrease in NHE6 gene expression was noted following Epstein-Barr virus infection[33]. While the full implications of diminished NHE6 expression following viral infection is not well understood, the fact that multiple disparate types of viral pathogens induce reductions in NHE6 strongly suggest that it plays an important role in viral

infections. While the mechanism behind how Vif downmodulates the 50 kDa form of NHE6 remains to be determined, it is possible that other viral proteins may also target NHE6 expression.

In contrast to NHE6, significant upregulation of *SLC9A9* expression, the gene encoding NHE9, has been observed in non-human primates challenged with several human-isolated strains of H5N1 avian flu viruses[34,35]. In addition, NHE9 mRNA was significantly increased in extracellular vesicles secreted from cells infected with West Nile virus[36]. These findings suggest that in addition to viral proteins specifically targeting NHEs, cells may also alter production of NHEs in response to infection. Future investigation of interplay between cellular induced changes in NHE expression and how this is altered by viral proteins would provide important insight into how changes in the pH of endosomal compartments combats viral infection.

Nef and V-ATPase. It is worth noting that Nef has been reported to interact with the H subunit of V-ATPase[37] and these interactions might be relevant to endosomal pH changes. Although this is of great interest and could suggest that Nef plays a role in acidification of some endosomal compartments, we have thus far been unable confirm the interaction between Nef and V-ATPase subunit H. Further, we found no Nef-dependent difference in acidification of transferrin$^+$ compartments.

Although significant work remains to fully understand the interplay between HIV-1 Nef, endosomal compartment acidification, and Vif-dependent NHE6 downmodulation, our findings provide novel insights into the role of transferrin$^+$ compartmental pH in Nef-dependent MHC-I trafficking. It also reveals a new and complex role for Vif in Nef-dependent MHC-I downmodulation.

RESOURCE AVAILABILITY

Lead contact

Further information and requests for resources and reagents should be directed to and will be fulfilled by the lead contact, Kathleen Collins, MD, PhD (klcollin@med.umich.edu).

Materials availability

All unique reagents generated in this study are available from the lead contact with a completed Materials Transfer Agreement.

Data and code availability

- All data generated and reported in this paper are available from the lead contact upon request.
- This paper does not report original code.
- Any additional information required to reanalyze the data reported in this work paper is available from the lead contact upon request.

ACKNOWLEDGEMENTS

This research was funded by NIH grants R01 AI148383 to K.L.C, 1 TL1 DK 136046-1 to M.E.Y.M. and T32AI007413 (to F.G.R.). F.G.R. was also supported by a supplement to NIH R01 AI148084 to KLC. G.G.F. was supported by the National Institute Of General Medical Sciences of the National Institutes of Health under Award Number T32GM149391. The content is solely the responsibility of the authors and does not necessarily represent the official views of the National Institutes of Health. The University of Michigan Flow Cytometry Core and the University of Michigan Microscopy Core provided access to instruments and technical support. Eurofins sequenced recombinant DNA constructs. We thank S.-J.-K. Yee (City of Hope National Medical Center) for providing pCMV-HIV-1. We thank Nancy Hopkins (Massachusetts Institute of Technology) for providing VSV-G. Figure 6A was created with BioRender.com. We would like to thank Matthew Huston for his help in characterizing the NHE overexpressing viruses in T cell lines. Additionally, we want to thank Mark Painter for his ideas regarding the role of NHEs in Nef-dependent MHC-I downmodulation.

AUTHOR CONTRIBUTIONS

M.E.Y.M. conducted experiments, analyzed data, and wrote the manuscript. G.G.F. conducted experiments, analyzed data, and assisted in writing the methods of the manuscript. G.E.Z. conducted experiments, analyzed data, and assisted in writing the methods section of manuscript. F.G.R. assisted in conducting experiments.

DECLARATION OF INTERESTS

The authors declare no competing interests.

FIGURES AND LEGENDS

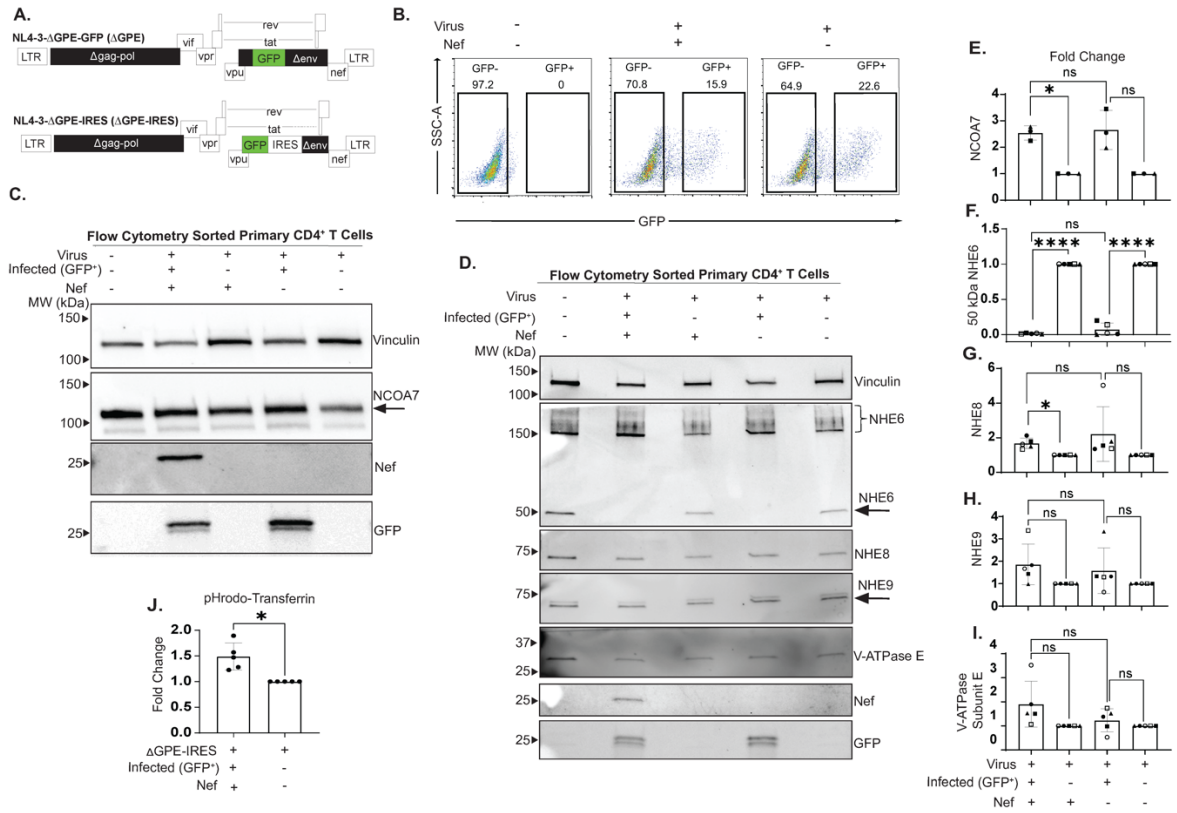

Figure 1. HIV-1 infection leads to striking reductions in the 50 kDa form of NHE6 expression, and enhanced acidification of intracellular compartments. (A) Schematic representation of viral genomes. Deleted genes are in black, HIV genes are in white, reporter genes are in green. (B) Representative flow plots of sorted primary CD4$^+$ T cells transduced with ΔGPE or ΔGPEN. GFP+ (transduced) and GFP- (untansduced) cells were sorted by fluorescence-activated cell sorting (FACS). Mock transduced samples were used as a control to set gates. See also Supplemental Figure S1A. (C) Lysates of sorted cells from (B) were subjected to western blot analysis. (D) Western blot analysis of lysates of primary CD4$^+$ T cells transduced with ΔGPE or ΔGPEN and sorted to isolate transduced and untransduced cells. See also Supplemental Figure S1B and C. (E) Summary graph of NCOA7 protein expression fold change of GFP+ and GFP- cells. Protein band intensities were quantified for 5 donors and normalized to vinculin. Fold change was then calculated by dividing the GFP+ vinculin-normalized signals by that of GFP-. (F) Summary graph of the 50 kDa NHE6 form protein expression fold change of GFP+ and GFP- cells. Fold change was calculated as described in (E). (G) Summary graph of NHE8 protein expression fold change of GFP+ and GFP- cells. Fold change was calculated as described in (E). (H) Summary graph of NHE9 protein expression fold change of GFP+ and GFP- cells. Fold change was calculated as described in (E). (I) Summary graph of V-ATPase protein expression fold change of GFP+ and GFP- cells. Fold change was calculated as described in (E). (J) Summary of fold change of transferrin$^+$ compartmental acidity in primary CD4$^+$ T cells transduced with ΔGPE-IRES shown in (A). Acidity of transferrin$^+$ compartments in GFP+ (transduced) and GFP- (untransduced) cells was evaluated by staining cells with pHrodo red-transferrin and AF-647-transferrin and subjecting to flow cytometry analysis. Fold change of pHrodo-red median fluorescence intensities (MFIs) normalized to AF-647 MFIs (to account for differences in transferrin uptake) was calculated relative to GFP- cells and graphed. 5 donors were evaluated. See also Supplemental Figure S1D. Statistical significance for (E) – (I) was determined with a One-Way ANOVA mixed effects model with Dunnett correction. Statistical significance for (J) was determined with a paired T-test. * $p < 0.05$, ** $p < 0.01$, *** $p < 0.001$, **** $p < 0.0001$.

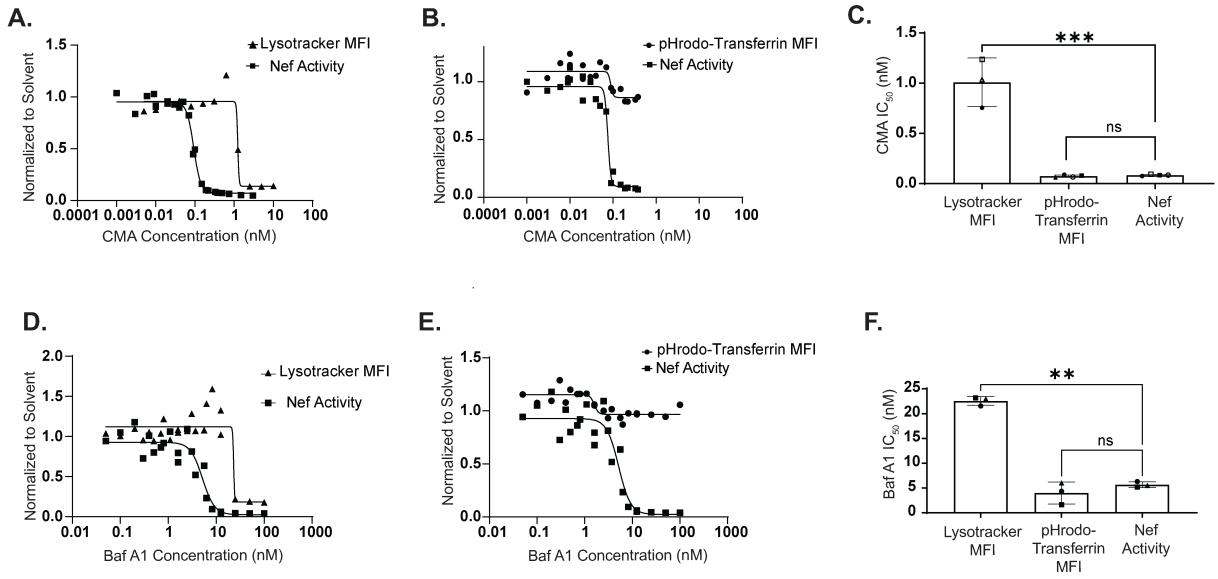

Figure 2. V-ATPase inhibitors neutralize transferrin$^+$ compartmental pH at concentrations that reverse Nef activity. (A) CMA dose response curves for primary CD4$^+$ T cells transduced with ΔGPE virus harboring FLAG-tagged Nef (ΔGPE FLAG-Nef) and treated with CMA or solvent two days after transduction for 24 hr. CMA concentrations ranged from 10 – 0.005 nM (Lysotracker MFI) or 3 – 0.001 nM (Nef Activity). (B) CMA dose response curves for primary CD4$^+$ T cells transduced with ΔGPE FLAG-Nef and treated with CMA or solvent two days after transduction for 24 hr then stained with pHrodo and AF-647 transferrin. CMA concentrations ranged from 0.38 – 0.001 nM. (C) Summary graphs of CMA IC_{50}s for Lysotracker MFI, pHrodo-transferrin MFI, and Nef activity. (D) Bafilomycin A1 (Baf A1) dose response curves for primary CD4$^+$ T cells transduced with ΔGPE FLAG-Nef and treated with Baf A1 or solvent two days after transduction for 24 hr. Baf A1 concentrations ranged from 100 – 0.05 nM. (E) Baf A1 dose response curves for primary CD4$^+$ T cells transduced with ΔGPE FLAG-Nef and treated with Baf A1 or solvent two days after transduction for 24 hr then stained with pHrodo and AF-647 transferrin. Baf A1 concentrations ranged from 100 – 0.05 nM. (F) Summary graphs of Baf A1 IC_{50}s for Lysotracker MFI, pHrodo-transferrin MFI, and Nef activity. Statistical significance for (C) and (F) was determined with a One-way ANOVA mixed effects analysis with Dunnett correction. * $p < 0.05$, ** $p < 0.01$, *** $p < 0.001$, **** $p < 0.0001$.

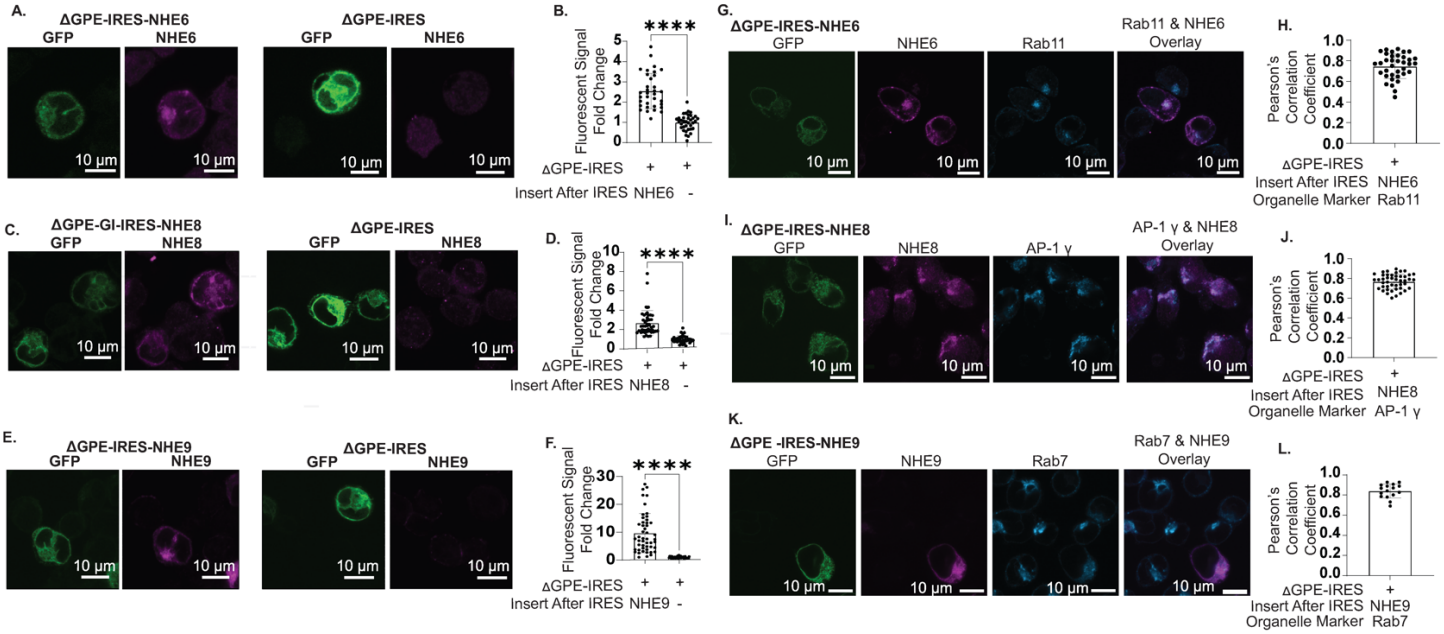

Figure 3. Viral constructs allow simultaneous HIV infection and NHE overexpression. (A) Representative fluorescence confocal microscopy images of CEM-A2 cells 48 hr after transduction with the indicated viruses and stained for NHE6. Identical laser settings were used for all images of each experimental replicate. (B) Summary graph of NHE6 expression 48 hr post transduction of CEM-A2 cells with the indicated viruses. Corrected total cell fluorescence (CTCF) was calculated for each cell. Fold change in NHE6 expression was calculated by dividing the CTCF of all cells by the average ΔGPE-IRES CTCF. At least 30 cells were imaged for each condition. (C) Representative images of CEM-A2 cells 48 hr after transduction with the indicated viruses and stained for NHE8. (D) Summary graph of NHE8 expression 48 hr post transduction of CEM-A2 cells with the indicated viruses. Fold change was calculated as described in (B). (E) Representative images of CEM-A2 cells 48 hr after transduction with the indicated viruses and stained for NHE9. (F) Summary graph of NHE9 expression 48 hr post transduction of CEM-A2 cells with the indicated viruses. Fold change was calculated as described in (B). See also Supplemental Figure S2A and B. (G) Representative images of NHE6 and Rab11 staining of CEM-A2 cells 48 hr post transduction with the indicated viruses. Organelle markers were imaged in the TRITC channel and pseudo-colored blue for easier visualization. (H) Summary graph of Pearson's correlation coefficient for overlap of signal between overexpressed NHE6 and Rab11. At least 16 cells were analyzed. (I) Representative images of NHE8 and AP-1 staining of CEM-A2 cells 48 hr post transduction with the indicated virus. (J) Summary graph of Pearson's correlation coefficient for overlap of signal between overexpressed NHE8 and AP-1. (K) Representative images of NHE9 and Rab7 staining of CEM-A2 cells 48 hr post transduction with the indicated virus. (L) Summary graph of Pearson's correlation coefficient for overlap of signal between overexpressed NHE9 and Rab7. See also Supplemental Figure S3A-C. Statistical significance for (B), (D), and (F) was determined with an unpaired T test. * $p < 0.05$, ** $p < 0.01$, *** $p < 0.001$, **** $p < 0.0001$.

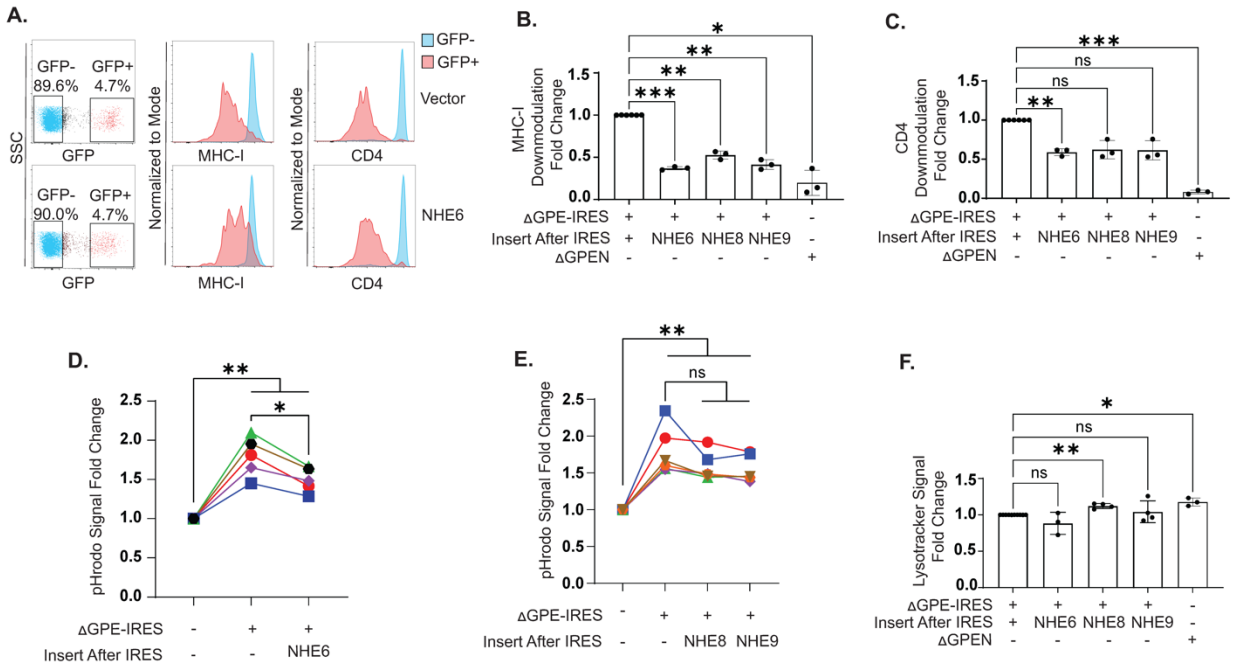

Figure 4. Overexpression of endosomal sodium/hydrogen exchangers reduces the ability of HIV-1 Nef to disrupt MHC-I trafficking. (A) Representative flow plots of primary CD4$^+$ T cells stained for surface MHC-I or CD4 expression 72 hr post transduction with the indicated viruses. (B) Summary graph of surface MHC-I expression in primary CD4$^+$ T cells 72 hr post transduction with the indicated viruses. MHC-I MFIs were obtained for GFP+ and GFP- cells. MHC-I downmodulation was calculated by dividing MHC-I MFIs of GFP+ cells by GFP- cells. The fold change was calculated by dividing the resulting values by that of the control virus (ΔGPE-IRES). 3 donors were evaluated. (C) Summary graph of Nef-dependent CD4 downmodulation in primary CD4$^+$ T cells 72 hr post transduction with the indicated viruses. CD4 downmodulation and fold change was calculated as described in (B), except CD4 MFIs were assessed. 3 donors were evaluated. (D) Summary graphs of transferrin$^+$ compartmental acidity of primary CD4$^+$ T cells 72 hr post transduction with the indicated viruses. Cells were stained with pHrodo-transferrin and AF-647-transferrin. Fold change in pHrodo signal was evaluated by dividing the pHrodo MFIs normalized to AF-647 MFIs of GFP+ cells by that of mock transduced cells. 5 donors were evaluated. (E) Summary graphs of transferrin$^+$ compartmental acidity of primary CD4$^+$ T cells 72 hr post transduction with the indicated viruses. Fold change was calculated as described in (D). See also Supplemental Figure S4A and B. (F) Summary graph of lysosome acidification in primary CD4$^+$ T cells 72 hr post transduction with the indicated viruses. Fold change was determined by dividing Lysotracker Red MFIs from GFP+ cells with Lysotracker Red MFIs from GFP+ cells transduced with the control virus (ΔGPE-IRES). 3 donors were evaluated. Statistical significance for (B), (C), and (F) was determined with a One-way ANOVA mixed effects analysis with Dunnett correction. Statistical significance for (D) and (E) was determined with a One-Way ANOVA mixed effect analysis with Tukey correction. * $p < 0.05$, ** $p < 0.01$, *** $p < 0.001$, **** $p < 0.0001$.

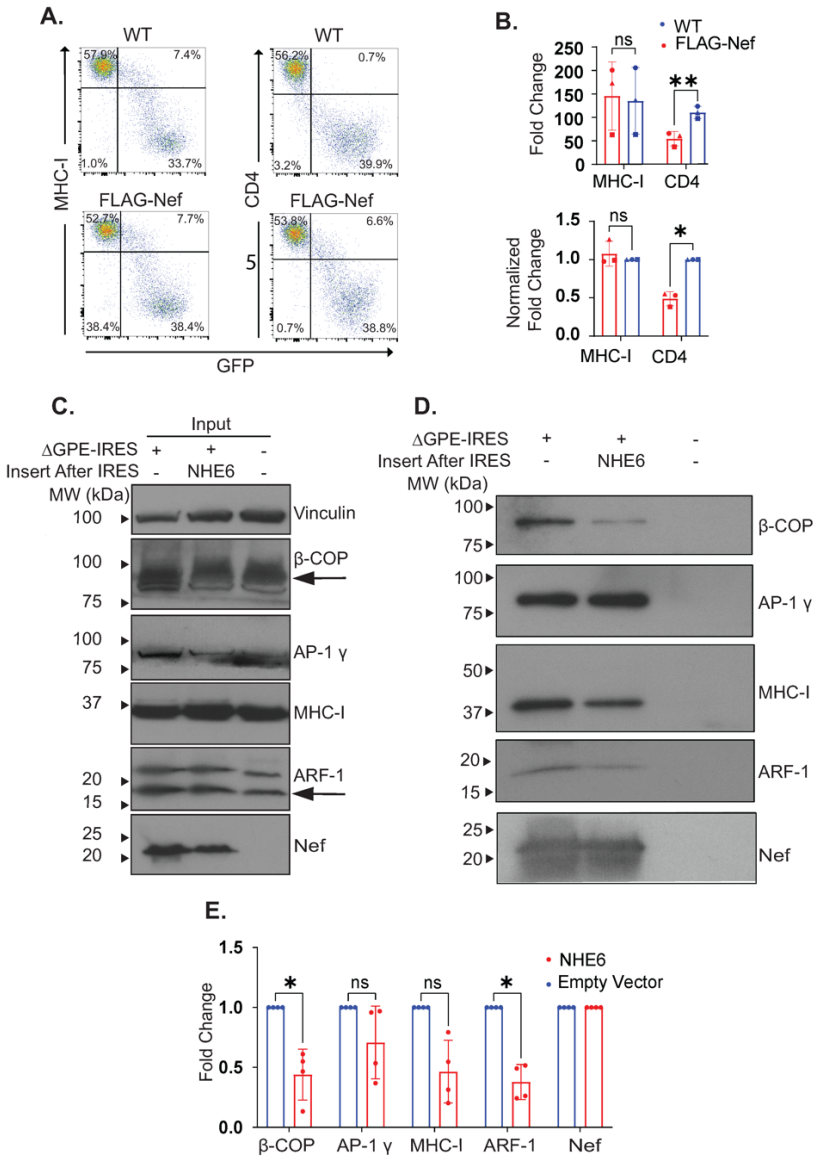

Figure 5. Neutralization of transferrin$^+$ compartments via NHE6 overexpression prevents Nef from binding to cellular proteins required for Nef-mediated disruption of MHC-I trafficking. (A) Representative flow plots showing MHC-I and CD4 downmodulation in CEM-A2 cells 48 hr post transduction with ΔGPE-IRES (WT) or ΔGPE-FLAG-Nef-IRES (FLAG-Nef). (B) Summary of fold change of CD4 and MHC-I downmodulation with or without the FLAG sequence inserted in Nef. Downmodulation was calculated as described in Figure 4B. To account for slight variation in the downmodulation between experimental replicates, MHC-I and CD4 downmodulation was normalized to WT Nef (bottom panel). 3 experimental replicates were performed (C) Representative western blot analysis of input (before incubation with FLAG beads) fractions of CEM-A2 lysates transduced with the indicated viruses. (D) Representative Co-IP western blot analysis of CEM-A2 cell lysates transduced with the indicated viruses. (E) Summary graphs of protein pulled down with Nef with or without NHE6 overexpression. Protein band signals were quantified and normalized to the Nef signal to account for slight differences in the amount of Nef pulled down between samples. Fold change of protein bound to Nef was calculated by dividing the Nef-normalized signals of NHE6-overexpressing samples by that of empty vector samples. 4 experimental replicates were performed. See also Supplemental Figure S4 C-E. Statistical significance was determined with a Paired T Test. * $p < 0.05$, ** $p < 0.01$, *** $p < 0.001$, **** $p < 0.0001$.

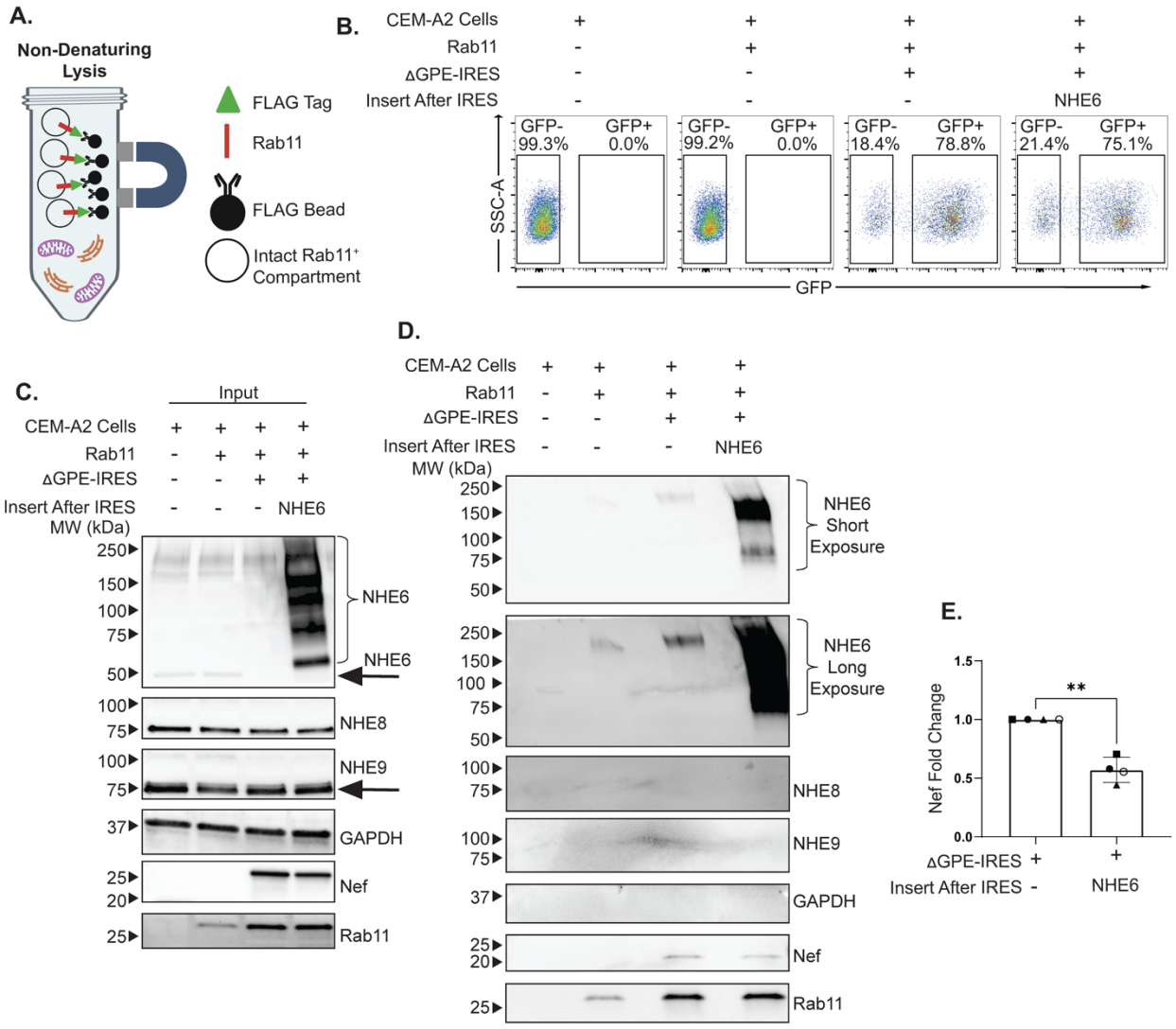

Figure 6. NHE6 overexpression disrupts recruitment of Nef to the recycling endosome. (A) Schematic diagram of the method to precipitate intact Rab11$^+$ compartments from CEM-A2 cells stably expressing FLAG-tagged Rab11 (CEM-A2-FLAG-Rab11). (B) Representative flow plots showing transduction rates of CEM-A2-FLAG-Rab11 cells 48 hr post transduction with the indicated viruses. (C) Representative western blot analysis of input (prior to incubation with FLAG beads) fractions of lysates from CEM-A2-FLAG-Rab11 cells 48 hr post transduction with the indicated viruses. (D) Representative Co-IP western blot analysis of isolated Rab11$^+$ compartments from CEM-A2-FLAG-Rab11 lysates transduced with the indicated viruses and precipitated with FLAG beads. (E) Summary graph of Nef expression in isolated Rab11$^+$ compartments during HIV-1 transduction with or without NHE6 overexpression. Nef signal was normalized to the Rab11 signal to account for slight variations in the amount of Rab11 pulled down. Fold change was then calculated by dividing the resulting value for NHE6 overexpressing samples by that of the control virus (ΔGPE-IRES) samples. 4 experimental replicates were performed. Statistical significance for (E) was determined with a paired T test. * $p < 0.05$, ** $p < 0.01$, *** $p < 0.001$, **** $p < 0.0001$.

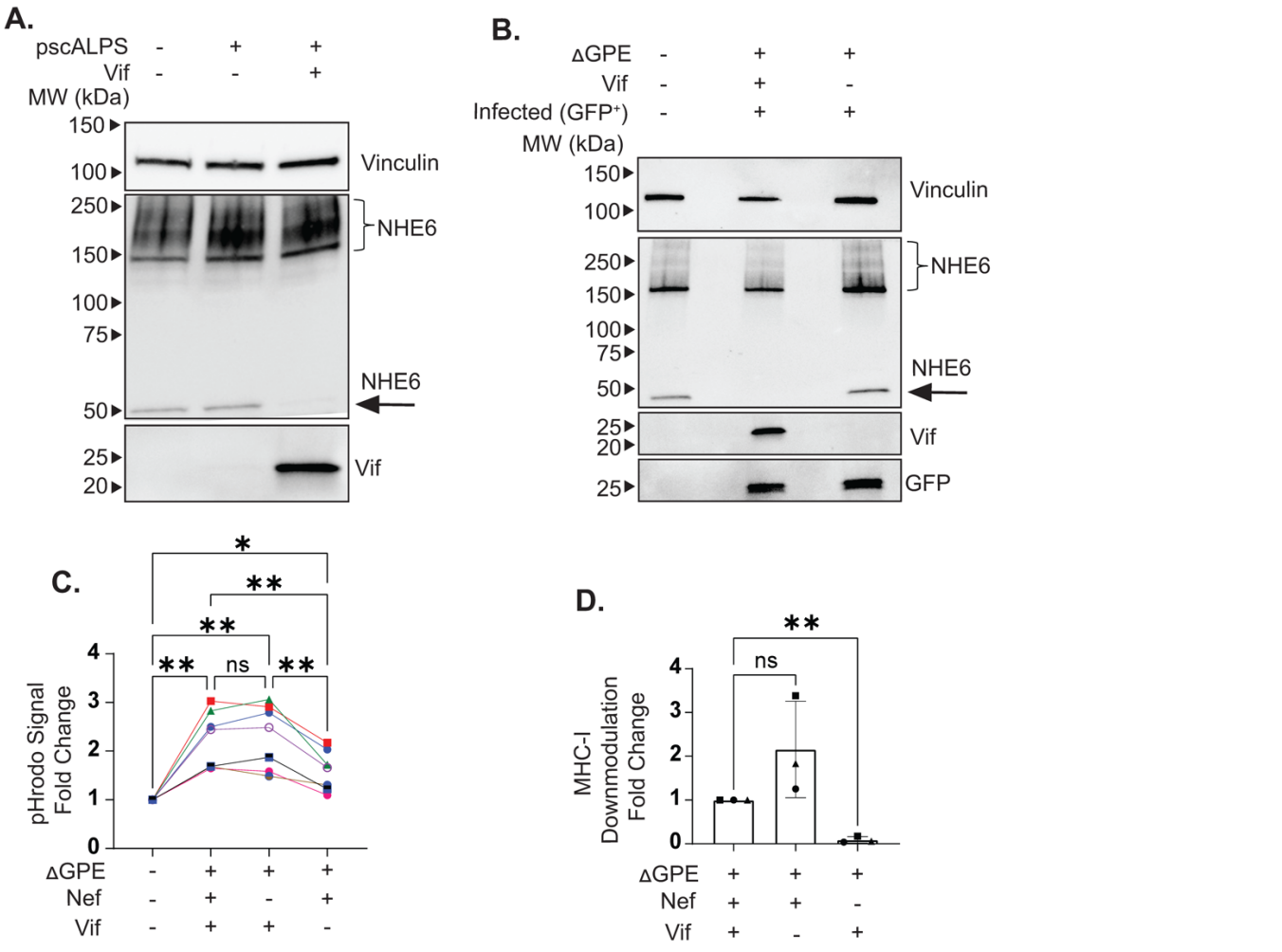

Figure 7. The HIV-1 accessory protein Vif downmodulates the 50 kDa form of NHE6 and contributes to acidification of transferrin$^+$ compartments. (A) Representative western blot analysis of CEM-A2 lysates transduced with pscALPS-Vif or an empty vector control and treated with puromycin for 3 days to isolate successfully transduced cells. (B) Representative western blot analysis of lysates from primary CD4$^+$ T cells transduced with the indicated viruses and sorted to isolate GFP+ (transduced) cells 48 hr post transduction. See also Supplemental Figure S5. (C) Summary graphs of transferrin$^+$ compartmental acidity of primary CD4$^+$ T cells 72 hr post transduction with the indicated viruses. Cells were stained with pHrodo-transferrin and AF-647-transferrin. Fold change in pHrodo signal was calculated as described in Figure 4D. 5 donors were evaluated. (D) Summary graph of surface MHC-I expression in primary CD4$^+$ T cells 72 hr post transduction with the indicated viruses. MHC-I downmodulation was calculated as described in Figure 4B. 3 donors were evaluated. Statistical significance for (C) was determined with a One-Way ANOVA mixed effects analysis with Tukey correction. Statistical significance for (D) was determined with a One-Way ANOVA mixed effects analysis with Dunnett correction. * $p < 0.05$, ** $p < 0.01$, *** $p < 0.001$, **** $p < 0.0001$.

STAR★Methods

Key resources table

.

REAGENT or RESOURCE	SOURCE	IDENTIFIER
Antibodies		
Monoclonal anti-HLA-A2 BB7.2	Umich hybridoma Core	N/A
Monoclonal anti-CD4 clone RPA-T4	BD Biosciences	Cat. 555344
Monoclonal anti-FLAG-HRP clone M2	Millipore Sigma	Cat. A8592-.2MG
Monoclonal anti-HA.11 Epitope Tag clone 16B12	BioLegend	Cat. 901513
Monoclonal anti-AP-1 γ clone 88	BD Biosciences	Cat. 610386
Monoclonal anti-Vinculin clone hVIN-1	Millipore Sigma	Cat. V9131-100UL
Polyclonal anti-β-COP	ThermoFisher Scientific	Cat. PA1-061
Polyclonal anti-ARF-1	ThermoFisher Scientific	Cat. PA1-127
Polyclonal anti-SLC9A6 (NHE6)	ThermoFisher Scientific	Cat. PA5-101894
Polyclonal anti-NHE8	Proteintech	Cat. 18318-1-AP
Polyclonal anti-SLC9A9 (NHE9)	ThermoFisher Scientific	Cat. PA5-42524
Monoclonal SLC9A9 Monoclonal Antibody (1B8D9) (NHE9) antibody	Proteintech	Cat. 66577-1-IG
Polyclonal anti-GFP	Abcam	Cat. Ab13970
Polyclonal anti-V-ATPase Subunit E1	Invitrogen	Cat. PA5-29899
Polyclonal anti-NCOA7	ProteinTech	Cat. 23092-1-AP
Monoclonal RAB11A Monoclonal Antibody 4H9	Invitrogen	Cat. MA5-49197
Monoclonal Rab7 (D95F2) XP® Rabbit antibody	Cell Signaling Technologies	Cat. 9367S
Monoclonal Anti-γ-Adaptin antibody produced in mouse	Sigma-Aldrich	Cat. A4200-.2ML
Monoclonal Anti-GAPDH antibody produced in mouse	Sigma-Aldrich	Cat. WH0002597M1-100UG
Polyclonal anti-HIV-1 Nef Protein	HIV Reagent Program	Cat. ARP-2949
Anti-Human Immunodeficiency Virus (HIV)-1 Vif Monoclonal Antibody	HIV Reagent Program	Cat. ARP-6459
Polyclonal Anti-Human Immunodeficiency Virus Type 1 NL4-3 Vpu Protein	HIV Reagent Program	Cat. ARP-969
Secondary goat anti-Mouse IgG2b , AlexaFluor 647	Fisher Scientific	Cat. A21242

Secondary goat anti-Mouse IgG1, PE	Fisher Scientific	Cat. P21129
Secondary goat anti-Mouse IgG1, AlexaFluor 546	Fisher Scientific	Cat. A21123
Secondary goat anti-Rabbit AlexaFluor 546	Fisher Scientific	Cat. A11035
Secondary goat anti-Rabbit AlexaFluor 647	Fisher Scientific	Cat. A21244
Goat anti-Mouse IgG2a Cross-Adsorbed Secondary Antibody, Alexa Fluor™ 647	ThermoFisher Scientific	Cat. A-21241
Goat anti-Mouse IgG2b Cross-Adsorbed Secondary Antibody, Alexa Fluor™ 488	ThermoFisher Scientific	Cat. A-21141
Goat anti-Rabbit HRP	Invitrogen	Cat. 65-6120
Goat anti-Mouse IgG-HRP	Invitrogen	Cat. 31430
Rat anti-Mouse IgG1-HRP clone M1-14012	eBioscience	Cat. 18-4015-82
Goat anti-Chicken IgY-HRP	Invitrogen	Cat. A16054
Bacterial and virus strains		
NEB Stable Competent E. coli	New England Biolabs	Cat. C3040H
ΔGPE FLAG-Nef	This paper	n/a
ΔGPE NL-GI-IRES	This paper	n/a
ΔGPE NL-GI-IRES-ARF-1	This paper	n/a
ΔGPE NL-GI-IRES-NHE6	This paper	n/a
ΔGPE NL-GI-IRES-NHE8	This paper	n/a
ΔGPE NL-GI-IRES-NHE9	This paper	n/a
ΔGPE NL-GI-FLAG-Nef-IRES-NHE6	This paper	n/a
ΔGPE NL-GI-FLAG-Nef-IRES	This paper	n/a
Biological samples		
Human PBMCs from blood donors	New York Blood Center	n/a
Human Serum, Type AB	Fisher Scientific	Cat. BP2525100
Goat Serum	Millipore Sigma	Cat. G9023
Chemicals, peptides, and recombinant proteins		
Gibco RPMI 1640 medium	Fisher Scientific	Cat. 11-875-093
Gibco DMEM medium	Fisher Scientific	Cat. 11-995-073
Gibco Fetal Bovine Serum	Fisher Scientific	Cat. 26140079
Invitrogen Penicillin/Streptomycin/Glutamine 100X	Fisher Scientific	Cat. 10-378-016
Plasmocin – Mycoplasma Elimination Reagent	InvivoGen	Cat. Ant-mpt
Invitrogen HEPES (1M)	Fisher Scientific	Cat. 15630080
Gibco Geneticin (G418 Sulfate) (50 mg/mL)	Fisher Scientific	Cat. 10131035
Puromycin Dihydrochloride	Sigma-Aldrich	Cat. P8833-25MG
Hexadimethrine Bromide (polybrene)	Millipore Sigma	Cat. H9268-5G
Lectin, PHA-L, *Phaseolus vulgaris*	Millipore Sigma	Cat. 431784-5MG
R&D Systems Recombinant Human IL-2 Protein	Fisher Scientific	Cat. 202IL010
Concanamycin A	Caymen Chemical	Cat. 11050
Bafilomycin A1	Caymen Chemical	Cat. 11038
Acetonitrile	Millipore Sigma	Cat. 34851-100ML
DMSO	Sigma Aldrich	Cat. D2650-5X5ML

DAPI solution (1 mg/mL)	ThermoFisher Scientific	Cat. EN62248
pHrodo Red Transferrin Conjugate	ThermoFisher Scientific	Cat. P35376
Invitrogen AlexaFluor 647 Transferrin Conjugate	ThermoFisher Scientific	Cat. T23366
Invitrogen Lysotracker Red DND-99	Fisher Scientific	Cat. L7528
16% Paraformaldehyde Aqueous Solution	Fisher Scientific	Cat. 50-980-487
Gibco PBS, pH7.4	Fisher Scientific	Cat. 10010049
Pierce IP Lysis Buffer	Fisher Scientific	Cat. P187787
cOmplete Mini Protease Inhibitor Cocktail Tablets	Millipore Sigma	Cat. 11836153001
Phenylmethylsulfonyl fluoride (PMSF)	Millipore Sigma	Cat. P7626
Halt™ Protease Inhibitor Cocktail (100X)	ThermoFisher Scientific	Cat. 87786
Anit-FLAG M2 Magnetic Beads	Millipore Sigma	Cat. M8823-5ML
3X FLAG Peptide	Millipore Sigma	Cat. F4799-4MG
4X Laemmli Sample Buffer	BioRad	Cat. 1610747
Polyethylenimine (PEI)	Polysciences Incorporated	Cat. 23966
BamHI Enzyme	New England BioLabs	Cat. R0136
EcoRI-HF Enzyme	New England BioLabs	Cat. R3101S
NotI-HF Enzyme	New England BioLabs	Cat. R3189S
XhoI Enzyme	New England BioLabs	Cat. R0146
SwaI Enzyme	New England BioLabs	Cat. R0604S
XbaI Enzyme	New England BioLabs	Cat. R0145
MluI Enzyme	New England BioLabs	Cat. R3198
BssHII Enzyme	New England BioLabs	Cat. R0199S
SalI Enzyne	New England BioLabs	Cat. R0138S
NheI-HF Enzyme	New England BioLabs	Cat. R3131S
T4 DNA Ligase	New England BioLabs	Cat. M0202
Corning Cell-Tak Cell and Tissue Adhesive	Fisher Scientific	Cat. CB-40241
Thermo Scientific Blocker BSA 10X in PBS	ThermoFisher Scientific	Cat. PI37525

NHE6 Antibody Epitope Peptide: LAFGDHELVIRGTRLVLPMDDSEPPLNLLDNTRH GPA	Biomatik	N/A custom ordered.
Critical commercial assays		
Invitrogen Dynabeads CD8	Fisher Scientific	Cat. 11147D
EndoFree Plasmid Maxiprep Kit	Qiagen	Cat. 12362
Pierce BCA Protein Assay Kit	ThermoFisher Scientific	Cat. 23227
Deposited data		
None was used in this manuscript		
Experimental models: Cell lines		
HEK 293T Cells	ATCC	Cat. CRL-3216
CEM-A2 cells (modified from CEM-SS cell line)	Collins Lab	n/a
Experimental models: Organisms/strains		
None were used in this manuscript		
Oligonucleotides		
NHE6 forward - GTA TCT AGA ACC AGG ATG GCT CGG AGA GGC TGG AG	IDT	n/a
NHE6 reverse - GTA ACG CGT TCA GGC GGG GCC GTG TCT TGT AT	IDT	n/a
NHE7 forward - GTA TCT AGA ACC AGG ATG GAG CCT GGC GAT GC	IDT	n/a
NHE7 reverse - GTA ACG CGT TCA GGC GTT GTC CTC CAG TGG	IDT	n/a
NHE8 forward - GTA TCT AGA ACC AGG ATG GGC GAG AAG ATG GCC	IDT	n/a
NHE8 reverse - GTA ACG CGT TCA CAG CAG CTC CTG CTC ATC G	IDT	n/a
NHE9 forward - GTA TCT AGA ACC AGG ATG GAG AGG CAG TCT CGC G	IDT	n/a
NHE9 reverse - GTA ACG CGT TCA ATT CAG CTG GCT CTG GCC C	IDT	n/a
NL-GI-EV-ΔGPE Forward – CTAGA-ACCGGT-ATCGAT-ACTAGT-A	IDT	n/a
NL-GI-EV-ΔGPE Reverse - CGCGT-ACTAGT-ATCGAT-ACCGGT-T	IDT	n/a
NL-GI-EV-ΔGPE Nef-FLAG Forward – AAC-GGA-TCC-TTA-GCA-CTT-ATC-TGG-G	IDT	n/a
NL-GI-EV-ΔGPE Nef-FLAG Reverse – GGT-CTC-GAG-ATA-CTG-CTC-CCA-C	IDT	n/a

Recombinant DNA		
pDONR221_SLC9A6	Addgene	132175
pDONR221_SLC9A8	Addgene	132199
pDONR221_SLC9A9	Addgene	132211
pHAGE-3FLAG-RAB11A	Addgene	176489
VSV.G	Nancy Hopkins, Massachusetts Institute of Technology	N/A
pCMV-HIV	DOI: 10.1128/JVI.73.3.1828-1834.1999	N/A
Software and algorithms		
Image Studio Software	LI-COR	Download: https://www.licor.com/bio/image-studio/
FlowJo version 10.8.1	Tree Star	Download: https://www.flowjo.com/solutions/flowjo/downloads
GraphPad Prism version 9.5.0	Graph Pad	Download: https://www.graphpad.com/features
ImageLab Software version 6.1	Bio-Rad	Download: https://www.bio-rad.com/en-us/product/image-lab-software?ID=KRE6P5E8Z
Fiji Image J Software	Open source	Download: https://imagej.net/software/fiji/downloads
Nikon Elements Advanced Research (AR) Software	Nikon	Download: https://www.microscope.healthcare.nikon.com/products/software/nis-elements/nis-elements-advanced-research

Other		
µ-Slide 8 Well Glass Bottom Chamber Slide	Ibidi	Cat. 80827
Nikon N-SIM + A1R confocal microscope	Nikon	N/A
ZE5 cell analyzer flow cytometer	Bio-Rad	Cat. 12004278
Bigfoot Spectral Cell Sorter	Thermo Fisher	N/A
Aurora spectral analyzer flow cytometer	Cytek	N/A
iBright CL750 Imaging System	ThermoFisher Scientific	Cat. A44116
ChemiDoc Imaging System	Bio-Rad	Cat. 12003153
Trans-Blot Turbo Transfer System	Bio-Rad	Cat. 1704150
Amicon Ultra-0.5 Centrifugal Filter Unit, 3 kDa, 0.5 mL	Millipore Sigma	Cat. UFC500324
4-15% Criterion Tris-HCl Protein Gel 12+2 well 45 µL	Bio-Rad	Cat. 3450027
4-15% Criterion TGX Protein Gel 12+2 well 45 µL	Bio-Rad	Cat. 6571083
Immobilon-P PVDF Membrane	Millipore Sigma	Cat. IPVH00010

Experimental model and study participant details

Cell lines and Primary Cells

All cells were maintained at 37 °C in 5% CO_2 humidified atmosphere. CEM cells engineered to express HA-tagged HLA-A2 (referred to as CEM-A2) were maintained in R10-Geneticin medium prepared as follows: RPMI 1640 medium (Fisher Scientific, USA) supplemented with Plasmocin (2.6 µg/mL, InvivoGen), 8.8 mM HEPES (Fisher Scientific), 0.87 U/mL Penicillin, 0.86 µg/mL streptomycin, 0.25 mg/mL L-glutamine (Penicillin-Streptomycin-Glutamine, Fisher Scientific), 10% fetal bovine serum (Fisher Scientific), and 0.95 mg/mL Geneticin (Fisher Scientific). Media was sterile filtered before use.

Frozen stocks of HLA-$A2^+$ peripheral blood mononuclear cells (PBMCs) obtained from ficoll of Leukopaks from New York Blood Center were thawed and rested in R10 medium (prepared as described above, except without geneticin) overnight. The following day, cells were CD8 depleted by washing the cells once in with MACs buffer (2% FBS and 1 mM EDTA in PBS), adding 25 µL CD8 Dynabeads (Fisher Scientific) per 10^6 PBMCs and washing twice with MACs buffer. PBMCs were resuspended at a density of 10^6 cells/mL and rotated with the washed CD8 Dynabeads at 4 °C for 30 minutes. The supernatant containing only $CD4^+$ cells was removed from the beads, pelleted, and resuspended in 20 mL of R10 supplemented with 5 µg/mL PHA (Millipore Sigma). The following day, 15 mL of media was removed from the flask and replaced with 5 mL

of R10 supplemented with 100 U/mL IL-2 (final IL-2 concentration in the flask was 50 U/mL, Fisher Scientific). 72 hours post-PHA treatment, cells were used for downstream assays as described.

HEK 293T cells (ATCC) were maintained in D10, which was prepared like R10 except with DMEM medium (Fisher scientific) and without HEPES.

Generation of a Stable Cell Line Expressing FLAG-Tagged Rab11A

Virus was prepared with pHAGE-3FLAG-RAB11A as described below. CEM-A2 cells were transduced with the virus as described below. 48 hours post transduction, cells were resuspended at a density of 500,000 cells/mL in R10-Geneticin + 1 µg/mL puromycin (Sigma-Aldrich). Viability was monitored every day for 3 days and then cells were split with R10-Geneticin + 1 µg/mL puromycin at a density of 200,000 cells/mL. Cells were maintained in this media for 5 passages and were then transferred into R10-Geneticin + 0.5 µg/mL puromycin for long-term culture. Cells were maintained in this media.

Method details

Cloning of ΔGPE-IRES-NHEs:

NL4.3-GFP-IRES-ARF-1-ΔE virus [25]was truncated to remove a section of the Gag-Pol gene by digesting with SwaI (NEB), gel purifying the truncated fragment and re-ligating to produce ΔGPE NL-GI-IRES-ARF-1. ARF-1 was then replaced with NHEs in ΔGPE NL-GI-IRES-ARF-1 using XbaI and MluI (NEB) cloning sites to obtain ΔGPE-IRES-NHE6/8/9. NHEs were obtained from Addgene (#132175, #132199, #132211). The following primers were used to amplify the NHE sequences and add the XbaI and MluI sites.

NHE6 forward - GTA TCT AGA ACC AGG ATG GCT CGG AGA GGC TGG AG

NHE6 reverse - GTA ACG CGT TCA GGC GGG GCC GTG TCT TGT AT

NHE8 forward - GTA TCT AGA ACC AGG ATG GGC GAG AAG ATG GCC

NHE8 reverse - GTA ACG CGT TCA CAG CAG CTC CTG CTC ATC G

NHE9 forward - GTA TCT AGA ACC AGG ATG GAG AGG CAG TCT CGC G

NHE9 reverse - GTA ACG CGT TCA ATT CAG CTG GCT CTG GCC C

ΔGPE NL-GI-IRES-ARF-1 and NHE inserts from PCR were double digested with XbaI and MluI. Following gel purification, digestion products were ligated according to the NEB ligation protocol

with T4 DNA Ligase, transformed into NEB Stable Competent E. coli, and confirmed by Sanger sequencing and restriction digest.

Cloning of ΔGPE-IRES:

Primers were designed to replace ARF-1 in ΔGPE NL-GI-IRES-ARF-1 with multiple cut sites (AgeI, ClaI, SpeI) rather than a protein of interest. The resulting construct is called ΔGPE NL-GI-IRES.

Forward – CTAGA-ACCGGT-ATCGAT-ACTAGT-A

Reverse - CGCGT-ACTAGT-ATCGAT-ACCGGT-T

Primers were annealed together and ligated with ΔGPE NL-GI-IRES-ARF-1 digested with XbaI and MluI then ligated after gel purification with T4 DNA ligase, following the NEB ligation protocol. The resulting product was transformed into NEB Stable Competent E. coli and confirmed by Sanger sequencing and restriction digest.

Cloning of ΔGPE-FLAG-Nef-IRES and ΔGPE-FLAG-Nef-IRES-NHE6:

The following primers were used for PCR to amplify FLAG tagged Nef from a synthetic gBlock construct:

Forward – AAC-GGA-TCC-TTA-GCA-CTT-ATC-TGG-G

Reverse – GGT-CTC-GAG-ATA-CTG-CTC-CCA-C

gBlock sequence:

AACGGATCCTTAGCACTTATCTGGGACGATCTGCGGAGCCTGTGCCTCTTCAGCTACCACC
GCTTGAGAGACTTACTCTTGATTGTAACGAGGATTGTGGAACTTCTGGGACGCAGGGGGT
GGGAAGCCCTCAAATATTGGTGGAATCTCCTACAGTATTGGAGTCAGGAACTAAAGAATAG
TGCTGTTAACTTGCTCAATGCCACAGCCATAGCAGTAGCTGAGGGGACAGATAGGGTTATA
GAAGTATTACAAGCAGCTTATAGAGCTATTCGCCACATACCTAGAAGAATAAGACAGGGCT
TGGAAAGGATTTTGCTATAAGATGGGTGGCAAGTGGTCAAAAAGTAGTGTGATTGGATGGC
CTGCTGTAAGGGAAAGAATGAGACGAGCTGAGCCAGCAGCAGATGGG**GACTACAAAGAC**
GATGACGACAAGGTGGGAGCAGTATCTCGAGacc (Bolded letters indicate FLAG sequence. Letters highlighted in yellow represent the start codon for Nef.)

ΔGPE-IRES-NHE6, ΔGPE-IRES, and the PCR product were digested with XhoI and BamHI (NEB), gel extracted, and the products were ligated according to NEB ligation protocol

with T4 DNA Ligase. The resulting product was transformed into NEB Stable Competent E. coli and confirmed by Sanger sequencing and restriction digest.

Cloning of ΔGPE FLAG-Nef:

A FLAG tag was inserted into the N-terminal flexible loop of Nef with the following synthetic gBlock sequence:

GGATCCTTAGCACTTATCTGGGACGATCTGCGGAGCCTGTGCCTCTTCAGCTACCACCGC
TTGAGAGACTTACTCTTGATTGTAACGAGGATTGTGGAACTTCTGGGACGCAGGGGGTGG
GAAGCCCTCAAATATTGGTGGAATCTCCTACAGTATTGGAGTCAGGAACTAAAGAATAGTG
CTGTTAACTTGCTCAATGCCACAGCCATAGCAGTAGCTGAGGGGACAGATAGGGTTATAGA
AGTATTACAAGCAGCTTATAGAGCTATTCGCCACATACCTAGAAGAATAAGACAGGGCTTG
GAAAGGATTTTGCTATAAGATGGGTGGCAAGTGGTCAAAAAGTAGTGTGATTGGATGGCCT
GCTGTAAGGGAAAGAATGAGACGAGCTGAGCCAGCA**GACTACAAAGACGATGACGACAA**
GGCAGATGGGGTGGGAGCAGTATCTCGAG (Bolded letters indicate FLAG sequence. Letters highlighted in yellow represent that start codon for Nef.)

The gblock and NL4.3 ΔGPE backbone were double digested with BamHI and XhoI (NEB). The digested products were then ligated with T4 DNA ligase following the NEB ligation protocol. The resulting product was transformed into NEB Stable competent E. coli and confirmed by Sanger sequencing and restriction digest.

Cloning of ΔGPEF

A mutated *vif* sequence was inserted into the ΔGPE backbone with the following synthetic gBlock sequence:

CGAAAGTAAAGCCAGAGGAGATCTCTCGACGCAGGACTCGGCTTGCTGAAGCGCGCACG
GCAAGAGGCGAGGGGCGGCGACTGGTGAGTACGCCAAAAATTTTGACTAGCGGAGGCTA
GAAGGAGAGAGATGGGTGCGAGAGCGTCGGTATTAAGCGGGGGAGAATTAGATAAATGG
GAAAAAATTCGGTTAAGGCCAGGGGGAAAGAAACAATATAAACTAAAACATATAGTATGGG
CAAGCAGGGAGCTAGAACGATTCGCAGTTAATCCTGGCCTTTTAGAGACATCAGAAGGCT
GTAGACAAATACTGGGACAGCTACAACCATCCCTTCAGACAGGATCAGAAGAACTTAGATC
ATTATATAATACAATAGCAGTCCTCTATTGTGTGCATCAAAGGATAGATGTAAAAGACACCA
AGGAAGCCTTAGATAAGATAGAGGAAGAGCAAAACAAAAGTAAGAAAAAGGCACAGCAAG
CAGCAGCTGACACAGGAAACAACAGCCAGGTCAGCCAAAATTACCCTATAGTGCAGAACC

TCCAGGGGCAAATGGTACATCAGGCCATATCACCTAGAACTTTAAATGCATGGGTAAAAGT
AGTAGAAGAGAAGGCTTTCAGCCCAGAAGTAATACCCATGTTTTCAGCATTATCAGAAGGA
GCCACCCCACAAGATTTAAATTACCCATACAAAAGGAAACATGGGAAGCATGGTGGACAGA
GTATTGGCAAGCCACCTGGATTCCTGAGTGGGAGTTTGTCAATACCCCTCCCTTAGTGAAG
TTATGGTACCAGTTAGAGAAAGAACCCATAATAGGAGCAGAAACTTTCTATGTAGATGGGG
CAGCCAATAGGGAAACTAAATTAGGAAAAGCAGGATATGTAACTGACAGAGGAAGACAAAA
AGTTGTCCCCCTAACGGACACAACAAATCAGAAGACTGAGTTACAAGCAATTCATCTAGCT
TTGCAGGATTCGGGATTAGAAGTAAACATAGTGACAGACTCACAATATGCATTGGGAATCA
TTCAAGCACAACCAGATAAGAGTGAATCAGAGTTAGTCAGTCAAATAATAGAGCAGTTAATA
AAAAAGGAAAAAGTCTACCTGGCATGGGTACCAGCACACAAAGGAATTGGAGGAAATGAA
CAAGTAGATAAATTGGTCAGTGCTGGAATCAGGAAAGTACTATTTTTAGATGGAATAGATAA
GGCCCAAGAAGAACATGAGAAATATCACAGTAATTGGAGAGCAATGGCTAGTGATTTTAAC
CTACCACCTGTAGTAGCAAAAGAAATAGTAGCCAGCTGTGATAAATGTCAGCTAAAAGGGG
AAGCCATGCATGGACAAGTAGACTGTAGCCCAGGAATATGGCAGCTAGATTGTACACATTT
AGAAGGAAAAGTTATCTTGGTAGCAGTTCATGTAGCCAGTGGATATATAGAAGCAGAAGTA
ATTCCAGCAGAGACAGGGCAAGAAACAGCATACTTCCTCTTAAAATTAGCAGGAAGATGGC
CAGTAAAAACAGTACATACAGACAATGGCAGCAATTTCACCAGTACTACAGTTAAGGCCGC
CTGTTGGTGGGCGGGGATCAAGCAGGAATTTGGCATTCCCTACAATCCCCAAAGTCAAGG
AGTAATAGAATCTATGAATAAAGAATTAAAGAAAATTATAGGACAGGTAAGAGATCAGGCTG
AACATCTTAAGACAGCAGTACAAATGGCAGTATTCATCCACAATTTTAAAAGAAAAGGGGG
GATTGGGGGGTACAGTGCAGGGGAAAGAATAGTAGACATAATAGCAACAGACATACAAAC
TAAAGAATTACAAAAACAAATTACAAAAATTCAAAATTTTCGGGTTTATTACAGGGACAGCA
GAGATCCAGTTTGGAAAGGACCAGCAAAGCTCCTCTGGAAAGGTGAAGGGGCAGTAGTAA
TACAAGATAATAGTGACATAAAAGTAGTGCCAAGAAGAAAAGCAAAGATCATCAGGGATT**G**
CAGAAAACAGATGGCAGGTG**GCA**ATTGTGTGGCAAGTAGACAGG**GCA**AGGATTAACACAT
GGAAAAGATTAGTAAAACACCAT**GCA**TATATTTCAAGGAAAGCTAAGGACTGGTTTTATAGA
CATCACTATGAAAGTACTAATCCAAAAATAAGTTCAGAAGTACACATCCCACTAGGGGATGC
TAAATTAGTAATAACAACATATTGGGGTCTGCATACAGGAGAAAGAGACTGGCATTTGGGT
CAGGGAGTCTCCATAGAATGGAGGAAAAAGAGATATAGCACACAAGTAGACCCTGACCTA
GCAGACCAACTAATTCATCTGCACTATTTTGATTGTTTTTCAGAATCTGCTATAAGAAATACC
ATATTAGGACGTATAGTTAGTCCTAGGTGTGAATATCAAGCAGGACATAACAAGGTAGGAT
CTCTACAGTACTTGGCACTAGCAGCATTAATAAAACCAAAACAGATAAAGCCACCTTTGCCT
AGTGTTAGGAAACTGACAGAGGACAGATGGAACAAGCCCCAGAAGACCAAGGGCCACAGA
GGGAGCCATACAATGAATGGACACTAGAGCTTTTAGAGGAACTTAAGAGTGAAGCTGTTAG

ACATTTTCCTAGGATATGGCTCCATAACTTAGGACAACATATCTATGAAACTTACGGGGATA CTTGGGCAGGAGTGGAAGCCATAATAAGAATTCTGCAACAACT (Bolded letters indicate Methionine to Alanine mutations.)

The gblock and NL4.3 ΔGPE backbone were digested with BssHII and followed by digestion with EcoRI (NEB). The digested products were gel purified, then ligated with T4 DNA ligase following the NEB ligation protocol. The resulting product was transformed into NEB Stable competent E. coli and confirmed by Sanger sequencing and restriction digest.

Cloning of ΔGPEU

A mutated *vpu* sequence was inserted into the ΔGPE backbone with the following synthetic gBlock sequence:

GGGTGTCGACATAGCAGAATAGGCGTTACTCGACAGAGGAGAGCAAGAAATGGAGCCAGT
AGATCCTAGACTAGAGCCCTGGAAGCATCCAGGAAGTCAGCCTAAAACTGCTTGTACCAAT
TGCTATTGTAAAAAGTGTTGCTTTCATTGCCAAGTTTGTTTCATGACAAAAGCCTTAGGCAT
CTCCTATGGCAGGAAGAAGCGGAGACAGCGACGAAGAGCTCATCAGAACAGTCAGACTCA
TCAAGCTTCTCTATCAAAGCAGTAAGTAGTACATGTA**GCC**CAACCTATAATAGTAGCAATAG
TAGCATTAGTAGTAGCAATAATAATAGCAATAGTTGTGTGGTCCATAGTAATCATAGAATAT
AGGAAAATATTAAGACAAAGAAAAATAGACAGGTTAATTGATAGACTAATAGAAAGAGCAGA
AGACAGTGGCAATGAGAGTGAAGGAGAAGTATCAGCACTTGTGGAGATGGGGGTGGAAAT
GGGGCACCATGCTCCTTGGGATATTGATGATCTGTAGTGCTACAGAAAAATTGTGGGTCAC
AGTCTATTATGGGGTACCTGTCGCCACCATGGTGAGCAAGGGCGAGGAGCTGTTCACCGG
GGTGGTGCCCATCCTGGTCGAGCTGGACGGCGACGTAAACGGCCACAAGTTCAGCGTGT
CCGGCGAGGGCGAGGGCGATGCCACCTACGGCAAGCTGACCCTGAAGTTCATCTGCACC
ACCGGCAAGCTGCCCGTGCCCTGGCCCACCCTCGTGACCACCCTGACCTACGGCGTGCA
GTGCTTCAGCCGCTACCCCGACCACATGAAGCAGCACGACTTCTTCAAGTCCGCCATGCC
CGAAGGCTACGTCCAGGAGCGCACCATCTTCTTCAAGGACGACGGCAACTACAAGACCCG
CGCCGAGGTGAAGTTCGAGGGCGACACCCTGGTGAACCGCATCGAGCTGAAGGGCATCG
ACTTCAAGGAGGACGGCAACATCCTGGGGCACAAGCTGGAGTACAACTACAACAGCCACA
ACGTCTATATCATGGCCGACAAGCAGAAGAACGGCATCAAGGTGAACTTCAAGATCCGCC
ACAACATCGAGGACGGCAGCGTGCAGCTCGCCGACCACTACCAGCAGAACACCCCCATC
GGCGACGGCCCCGTGCTGCTGCCCGACAACCACTACCTGAGCACCCAGTCCGCCCTGAG
CAAAGACCCCAACGAGAAGCGCGATCACATGGTCCTGCTGGAGTTCGTGACCGCCGCCG

GGATCACTCTCGGCATGGACGAGCTGTACAAGGACGAGCTGTAAGCTAGCAAA (Bolded letters indicate Methionine to Alanine mutation)

The gblock and NL4.3 ΔGPE backbone were double digested with SalI and NheI (NEB). The digested products then ligated following gel purification with T4 DNA ligase following the NEB ligation protocol. The resulting product was transformed into NEB Stable competent E. coli and confirmed by Sanger sequencing and restriction digest.

Cloning of pscALPS-Vif.

The *vif* sequence was inserted into the pscALPs backbone with the following synthetic gBlock sequence:

ATCGTAGCTAGCTCTAGACTCGAGGCCACC**ATGGAAAACAGATGGCAGGTGATGATTGTG**
TGGCAAGTAGACAGGATGAGGATTAACACATGGAAAAGATTAGTAAAACACCATATGTA
TATTTCAAGGAAAGCTAAGGACTGGTTTTATAGACATCACTATGAAAGTACTAATCCAAA
AATAAGTTCAGAAGTACACATCCCACTAGGGGATGCTAAATTAGTAATAACAACATATTG
GGGTCTGCATACAGGAGAAAGAGACTGGCATTTGGGTCAGGGAGTCTCCATAGAATGGA
GGAAAAAGAGATATAGCACACAAGTAGACCCTGACCTAGCAGACCAACTAATTCATCTG
CACTATTTTGATTGTTTTTCAGAATCTGCTATAAGAAATACCATATTAGGACGTATAGTTA
GTCCTAGGTGTGAATATCAAGCAGGACATAACAAGGTAGGATCTCTACAGTACTTGGCA
CTAGCAGCATTAATAAAACCAAAACAGATAAAGCCACCTTTGCCTAGTGTTAGGAAACTG
ACAGAGGACAGATGGAACAAGCCCCAGAAGACCAAGGGCCACAGAGGGAGCCATACA
ATGAATGGACACTAGGAATTCGCTAGATCAT (Bolded Letters indicate *vif* sequence)

The gBlock and pscALPs backbone were double digested with XhoI and EcoRI (NEB). The digested products were gel purified, then ligated with T4 DNA ligase following the NEB ligation protocol. The resulting product was transformed into NEB Stable competent E. coli and confirmed by Sanger sequencing and restriction digest.

Cloning of LeGo BFP NHE6-FLAG

C-terminal FLAG-tagged NHE6 was inserted into a LeGo-iBFP expression vector with the following synthetic gblock sequence:

TGGTGGTACGGGAATTCATGGCTCGGAGAGGCTGGAGGCGCGCCCCTCTGCGGAGAGGA
GTGGGAAGCTCCCCTAGGGCAAGGCGCCTGATGAGACCACTGTGGCTGCTGCTGGCAGT
GGGCGTGTTCGATTGGGCAGGAGCATCTGACGGAGGAGGAGGAGAGGCCCGGGCCATG
GATGAGGAGATCGTGAGCGAGAAGCAGGCCGAGGAGTCCCACAGACAGGACTCTGCCAA

TCTGCTGATCTTCATCCTGCTGCTGACACTGACCATCCTGACCATCTGGCTGTTTAAGCAC
CGGAGAGCCAGGTTCCTGCACGAGACAGGCCTGGCCATGATCTACGGACTGCTGGTGGG
ACTGGTGCTGCGCTATGGCATCCACGTGCCATCCGATGTGAACAATGTGACCCTGTCTTG
CGAGGTGCAGTCTAGCCCCACCACACTGCTGGTGACATTCGACCCTGAGGTGTTCTTTAAT
ATCCTGCTGCCCCCTATCATCTTTTACGCCGGCTATTCCCTGAAGAGGCGCCACTTCTTTC
GGAACCTGGGCTCTATCCTGGCCTACGCCTTTCTGGGCACCGCCATCAGCTGCTTCGTGA
TCGGCTCCATCATGTATGGCTGCGTGACCCTGATGAAGGTGACCGGCCAGCTGGCCGGC
GATTTCTACTTTACCGACTGTCTGCTGTTCGGCGCCATCGTGTCCGCCACAGATCCAGTGA
CCGTGCTGGCCATCTTCCACGAGCTGCAGGTGGACGTGGAGCTGTATGCCCTGCTGTTTG
GCGAGAGCGTGCTGAATGACGCCGTGGCCATCGTGCTGTCCTCTAGCATCGTGGCATACC
AGCCAGCAGGCGATAACTCTCACACATTTGACGTGACCGCCATGTTCAAGAGCATCGGCA
TCTTCCTGGGCATCTTTTCTGGCAGCTTCGCCATGGGAGCAGCAACAGGAGTGGTGACCG
CCCTGGTGACAAAGTTTACCAAGCTGAGGGAGTTCCAGCTGCTGGAGACAGGCCTGTTCT
TTCTGATGTCCTGGTCTACCTTTCTGCTGGCAGAGGCATGGGGCTTCACAGGAGTGGTGG
CCGTGCTGTTTTGCGGCATCACACAGGCCCACTACACCTATAACAATCTGAGCACAGAGTC
CCAGCACCGCACCAAGCAGCTGTTTGAGCTGCTGAACTTCCTGGCCGAGAATTTCATCTTT
TCCTATATGGGCCTGACACTGTTCACCTTTCAGAACCACGTGTTTAATCCTACCTTCGTGGT
GGGCGCCTTTGTGGCCATCTTCCTGGGCAGGGCCGCCAACATCTACCCACTGAGCCTGCT
GCTGAATCTGGGCCGGAGATCTAAGATCGGCAGCAATTTTCAGCACATGATGATGTTCGCA
GGACTGAGGGGAGCAATGGCCTTCGCCCTGGCCATCAGGGATACAGCCACCTACGCCCG
CCAGATGATGTTCTCCACCACACTGCTGATCGTGTTCTTTACCGTGTGGGTGTTTGGAGGA
GGAACCACAGCAATGCTGAGCTGCCTGCACATCCGGGTGGGCGTGGATTCCGACCAGGA
GCACCTGGGAGTGCCAGAGAACGAGAGGAGGACCACAAAGGCAGAGTCCGCCTGGCTGT
TTAGAATGTGGTACAACTTCGACCACAATTATCTGAAGCCACTGCTGACCCACTCTGGACC
ACCACTGACCACAACCCTGCCAGCATGCTGTGGACCTATCGCAAGATGTCTGACCAGCCC
TCAGGCCTATGAGAACCAGGAGCAGCTGAAGGACGATGACTCCGATCTGATCCTGAATGA
TGGCGACATCTCTCTGACCTACGGCGACAGCACAGTGAACACCGAGCCAGCCACATCCTC
TGCCCCACGGAGATTCATGGGCAACAGCTCCGAGGATGCACTGGACAGGGAGCTGGCCT
TTGGCGATCACGAGCTGGTCATCAGGGGAACCAGGCTGGTGCTGCCAATGGATGACAGC
GAGCCTCCACTGAACCTGCTGGACAATACAAGACACGGCCCCGCC**GACTACAAAGACGA**
TGACGACAAGTGAGCGGCCGCTACGTAAATTCC (Bolded letters indicated FLAG sequence).

The gblock and LeGo-iBFP backbone were double digested with EcoRI and NotI (NEB). The digested products were then ligated following gel purification with T4 DNA ligase following

the NEB ligation protocol. The resulting product was transformed into NEB Stable competent E. coli and confirmed by Sanger sequencing and restriction digest.

Virus Production

2 million HEK 293T cells were plated on a 10 cm dish and adhered overnight. The following day, 4 µg of VSV-G plasmid, 4 µg of pCMV-HIV plasmid, and 4 µg of the viral genome of interest were diluted in 952 µL of 150 mM NaCl. 48 µL of a 1 mg/mL stock of polyethylenimine (PEI, Polyscience Incorporated) was added to the solution and this was gently vortexed. The transfection solution incubated at room temperature for 15 minutes and 1 mL was added to the plate of cells. The transfection solution was scaled accordingly to facilitate transfection of multiple plates at once. Cells incubated with the transfection solution for 16 hours. The media was then aspirated and replaced with fresh D10. 48 hours post-transfection, media containing the virus was pelleted to remove dead cells and aliquots were frozen at -80 °C until use. All viruses were titrated with CEM-A2 cells to determine volumes of virus required for desired infection rates.

Viral Transductions

CEM-A2 cells were resuspended in virus diluted in D10 to achieve the desired infection rate at a density of 1 million cells/mL. 1 mL or 500 µL of cells was added to the wells of 24 or 48-well plate (0.5- 1 million cells/well). Cells centrifuged at 2,500 rpm for 2 hours at room temperature. Media was then aspirated and replaced with 1-2 mL of R10. Cells were cultured for 48-72 hours depending on the downstream application.

Primary $CD4^+$ T cells were transduced as described above in a 24-well plate, except 4 µg/mL of polybrene (Millipore Sigma) was added to the virus diluted in D10. After the centrifugation step, media was aspirated and replaced with 1 mL of R10 supplemented with 50 U/mL of IL-2 (Fisher Scientific).

Fluorescence Confocal Microscopy

A 0.02 µg/µL stock of Cell-Tak (Fisher Scientific) was prepared by diluting a stock solution in sterile 0.1 M sodium bicarbonate buffer, pH 8.0. 3.9 µg of Cell-tak was added to the wells of an 8-chamber glass coverslip (Ibidi) and incubated at room temperature for 20 minutes. The solution was aspirated, and wells were washed once with sterile water. The coverslip airdried at room temperature and when necessary, was wrapped in parafilm and stored overnight at 4 °C.

Antibodies used for Confocal Microscopy. Primary antibodies were diluted in 2% BSA (paraformaldehyde fixation described below) or 1% BSA (ethanol fixation described below). We

utilized antibodies directed toward NHE6 (ThermoFisher Scientific diluted 1:100), NHE8 (ProteinTech, diluted 1:50), NHE9 (Thermofisher Scientific, diluted 1:50 or ProteinTech diluted 1:100), Rab11A (Invitrogen, diluted 1:100), AP-1 γ (Sigma Aldrich, diluted 1:200), and Rab7 (Cell Signaling Technologies, diluted 1:100). Secondary antibodies were diluted 1:250 in 2% BSA (for paraformaldehyde fixation described below) or 1:200 in 1% BSA (for ethanol fixation described below). For detection of NHE6, NHE8, NHE9 (ThermoFisher Scientific), and Rab7 we utilized goat anti-rabbit AF-647 (Fisher Scientific) or goat anti-rabbit AF-546 (Fisher Scientific) secondary antibodies. For detection of NHE9 (ProteinTech) we utilized a goat anti-mouse IgG2a AF-647 (ThermoFisher Scientific) secondary antibody. For detection of Rab11A and AP-1 γ we utilized goat anti-mouse IgG2b AF-647 (ThermoFisher Scientific), goat anti-mouse IgG2b AF-488 (ThermoFisher Scientific), or goat anti-mouse IgG2b AF-546 (Fisher Scientific).

Transferrin uptake. Cells plated in a round bottom plate were washed once with Live Cell Imaging Buffer (LCIB, 140 mM NaCl, 2.5 mM KCl, 1.8 mM $CaCl_2$, 1.0 mM $MgCl_2$, 20 mM HEPES, pH 7.4 supplemented with 1% BSA right before use). Transferrin conjugated to AlexaFluor 647 (ThermoFisher Scientific) was diluted 1:200 in LCIB and incubated with the cells at 37 °C for 15 minutes. Cells were pelleted and washed once with LCIB. Cells were then subjected to paraformaldehyde fixation and antibody staining described below.

Paraformaldehyde fixation (NHE6 and Rab11 staining). Cells were fixed by adding 2% paraformaldehyde in PBS (PFA, Fisher Scientific) and incubating at room temperature for 20 minutes. Cells were permeabilized with 0.2% tween20 in PBS for 20 minutes at 37 °C, pelleted and washed once with 2% BSA in PBS. For the antibody staining step, cells were first pre-incubated on ice for 30 minutes with 2% BSA in PBS. Then, antibodies were diluted in 2% BSA in PBS as described above, added to the cells and were incubated for 20 minutes on ice. Cells were then pelleted and washed once with 2% BSA. Then, secondary antibodies were diluted in 2% BSA as described above, added to the cells, and were incubated on ice for 20 minutes, protected from light. Cells were then pelleted and washed once with 2% BSA. Nuclei were labeled by diluting a 1 mg/mL DAPI stock (ThermoFisher Scientific) 1:1,000 in PBS and incubating with the cells for 5 minutes at room temperature. Cells were washed once with 2% BSA, then resuspended in 200 µL 2% BSA and added to the wells of the cell-Tak coated 8-well chamber coverslip. Cells were adhered to the coverslip for 30 minutes at room temperature.

Ethanol fixation (NHE8 and NHE9 staining and colocalization of NHE8 with AP-1 or NHE9 with Rab7). Cells were resuspended in PBS at a density of 1,750 cells/µL and 200 µL was added to the wells of a cell-Tak coated coverslip (350,000 cells/well). Cells adhered to the

coverslip for 20 minutes at 37 °C and were fixed by adding ice-cold 100% ethanol to the wells and incubating at room temperature for 10 minutes. Ethanol was aspirated and cells were washed 3 times with PBS. Cells were permeabilized by adding 0.2% tween20 in PBS and incubating for 5 minutes at room temperature. Cells were washed 3 times with PBS. Prior to antibody staining, cells were preincubated with 5% goat serum (Millipore Sigma) in PBS for detecting overexpression of NHE8 and NHE9 or 2% BSA to monitor colocalization of NHE8 with AP-1 or NHE9 with Rab7 for 1 hour at room temperature. Then, primary antibodies described above were diluted in 1% BSA in PBS and incubated with the cells for 2.5 hours at room temperature with gentle rocking. The antibodies were then aspirated, and cells were washed three times with PBS with rocking for 5 minutes at room temperature. Secondaries were diluted 1:200 in 1% BSA as described above and incubated with the cells for 1.5 hours at room temperature with gentle rocking, protected from light. The secondary was aspirated, and cells were washed three times with PBS with rocking for 5 minutes at room temperature. Nuclei were stained with DAPI as described above. Cells were washed once with PBS and 200 µL of PBS was added to each well.

Imaging. Slides were imaged with a Nikon N-SIM + A1R confocal microscope. Identical laser and gain settings were used across all images for each replicate of the experiment.

Flow Cytometry Staining

Nef-dependent MHC-I and/or CD4 downmodulation from the cell surface in response to all viral transductions was evaluated by flow cytometric analysis of transduced primary T cells. Cells were stained in a round bottom 96-well plate 72 hours post transduction. Surface expression of MHC-I and/or CD4 was monitored using antibodies directed against HLA-A2 (BB7.2, Umich Hybridoma Core, 1:2,000 dilution) and CD4 (BD Biosciences 1:500 dilution). All antibodies were diluted in FACS buffer (2% FBS, 1% human serum, 10 mM HEPES, and 0.025% sodium azide in PBS). The antibody cocktail was added to the cells and incubated on ice for 20 minutes. Cells were pelleted and washed once with FACS buffer prior to incubation with secondary antibodies [goat anti-mouse IgG2b AF-647 (to detect BB7.2, Fisher Scientific) and goat anti-mouse IgG1 PE (to detect CD4, Fisher scientific)] diluted 1:2,000 in FACS buffer. DAPI was added as a viability dye to the secondary antibody cocktail at a final concentration of 0.04 µg/mL. Cells were incubated with the cocktail for 20 minutes on ice, protected from light. Cells were washed once with FACS buffer and fixed by adding 2% PFA to the wells and incubating for 20 minutes at room temperature, protected from light. Cells were resuspended in FACS buffer and analyzed on a ZE5 cell analyzer (Bio-Rad) or an Aurora spectral analyzer (Cytek). A minimum of 10,000 live events

were collected for each sample. All laser and gain settings were identical for all samples for each individual replicate of the experiment.

Changes in primary $CD4^+$ T cell transferrin$^+$ compartment pH in response to viral transduction were monitored 72 hours post-transduction with the indicated viruses. Cells were washed once with LCIB. Transferrin conjugated to pHrodo Red or AF-647 (ThermoFisher Scientific) was diluted 1:200 in LCIB and added to the wells. Cells were incubated for 15 minutes at 37 °C, pelleted and washed once with LCIB. Cells were resuspended in LCIB and analyzed without fixing on a ZE5 cell analyzer (Bio-Rad) or an Aurora spectral analyzer (Cytek). Laser and gain settings were identical for all samples for each individual replicate of the experiment.

To monitor neutralization of transferrin$^+$ compartments in response to CMA or Bafilomycin A1 treatment, primary $CD4^+$ T cells transduced with the indicated viruses and dosed with CMA (described below) or Bafilomycin A1 (described below) were pelleted in a round bottom 96-well plate 24 hours post compound treatment and stained exactly as described above.

To monitor neutralization of the lysosome in response to CMA or Bafilomycin A1 treatment or viral transduction, transduced primary $CD4^+$ T cells treated with or without the compounds were collected for staining 72 hours post transduction in a 96-well round bottom plate. Lysotracker Red (Fisher Scientific) diluted 1:5,000 in PBS was added and cells were incubated for 1 hour at 37 °C. Cells were then pelleted and washed once with FACS buffer. DAPI diluted to a final concentration of 0.04 µg/mL in FACS buffer was added to the cells and incubated 5 minutes at room temperature, protected from light. Cells were pelleted and washed once with FACS buffer. Cells were fixed by adding 2% PFA in PBS and incubating at room temperature for 20 minutes. Cells were resuspended in FACS buffer and analyzed with a ZE5 cell analyzer (Bio-Rad) or an Aurora spectral analyzer (Cytek). Laser and gain settings were identical for all samples for each individual replicate of the experiment.

CMA Titrations

Primary HLA-$A2^+$ $CD4^+$ T cells were isolated as described above. 72 hours post PHA treatment, cells were transduced with ΔGPE FLAG-Nef virus as described in the viral transduction section. 2 days post transduction, cells were resuspended at a density of 2 million cells/mL in R10 + 100 U/mL IL-2. 50 µL of the cell suspension was added to the wells of a flat-bottom 96-well plate (100,000 cells/well). Two titrations of CMA were performed. For the first titration, CMA (Caymen chemical) was diluted in R10 to produce a 1.5 nM stock and acetonitrile (Millipore Sigma) was diluted the same way to produce a solvent control. CMA and acetonitrile were serial

diluted 1:1 in R10 to produce concentrations ranging from 0.75 – 0.0029 nM. In an effort to obtain more data points near the IC_{50} for transferrin conjugated to pHrodo Red signal (indicative of transferrin$^+$ compartment neutralization) a second titration of CMA and acetonitrile was prepared in which a 0.67 nM CMA stock was prepared in R10. This stock or acetonitrile was serial diluted 1:1.5 in R10 to produce a range of CMA concentrations from 0.33 – 0.017 nM. 50 µL of each CMA or acetonitrile concentration was added to the cells. Final media volume was 100 µL/well with 100,000 cells/well. For the first CMA titration, the final range of CMA concentrations was 0.38 nM – 0.001 nM. The final range of concentrations for the second CMA titration was 0.33 nM – 0.009 nM. The final IL-2 concentration was 50 U/mL. Cells were incubated with CMA for 24 hours and then stained for flow cytometric analysis of MHC-I expression and transferrin$^+$ compartment neutralization as described above.

Since neutralization of the lysosome occurs at substantially higher concentrations of CMA than required to reverse Nef-dependent MHC-I downmodulation and neutralize transferrin$^+$ compartments, a separate CMA titration was performed starting a higher concentration. Primary CD4$^+$ were transduced with ΔGPE FLAG-Nef and added to the flat-bottom 96-well plate as descried above. CMA (Caymen Chemical) was diluted to produce a 20 nM stock in R10 and acetonitrile was diluted the same way to produce a solvent control. This stock and the acetonitrile were serial diluted 1:1 to produce concentrations of CMA ranging from 20 – 0.01 nM. CMA or acetonitrile at each concentration was added to the cells. The final volume in the wells was 100 µL with 100,000 cells/well. The final range of CMA concentrations was 10 – 0.005 nM. The final IL-2 concentration in the wells was 50 U/mL. Cells were incubated with CMA for 24 hours prior to staining with lysotracker as described above.

Bafilomycin A1 Titrations

Primary HLA-A2$^+$ CD4$^+$ T cells were isolated as described above. 72 hours post PHA treatment, cells were transduced with ΔGPE FLAG-Nef virus as described in the viral transduction section. 2 days post transduction, cells were resuspended at a density of 2 million cells/mL in R10 + 100 U IL-2/mL. 50 µL of the cell suspension was added to the wells of a flat-bottom 96-well plate (100,000 cells/well). Two titrations of Bafilomycin A1 (Baf A1) were performed. For the first titration, Baf A1 (Caymen chemical) was diluted in R10 to produce a 200 nM stock and DMSO (Sigma Aldrich) was diluted the same way as a solvent control. Baf A1 and DMSO were serial diluted 1:1 in R10 to produce concentrations ranging from 200 – 0.1 nM. In an effort to obtain more data points near the IC_{50} for transferrin conjugated to pHrodo Red signal (indicative of transferrin$^+$ compartment neutralization) a second titration of Baf A1 and DMSO was prepared in

which a 25 nM stock was prepared in R10. This stock or DMSO was serial diluted 1:1.5 in R10 to produce a range of Baf A1 concentrations from 25 – 0.6 nM. 50 µL of each Baf A1 or DMSO concentration was added to the cells. Final media volume was 100 µL/well with 100,000 cells/well. For the first Baf A1 titration, the final range of Baf A1 concentrations was 100 nM – 0.05 nM. The final range of concentrations for the second Baf A1 titration was 12.5 nM – 0.3 nM. The final IL-2 concentration was 50 U/mL. Cells incubated with Baf A1 for 24 hours and were then stained for flow cytometric analysis of MHC-I downmodulation, transferrin^{+} compartment neutralization, and lysotracker as described above.

Fluorescence-Activated Cell Sorting (FACS)

For all sorting experiments, cells were collected 48 hours post transduction and resuspended at a density of 5,000,000 cell/mL in MACs buffer. Cells were sorted based on GFP expression with a Bigfoot Spectral Cell Sorter (ThermoFisher Scientific) into tubes containing R10.

Western Blot Analysis

Lysate preparation, SDS PAGE and transfer. Sorted cells or lentiviral transduced cells selected in puromycin were washed once with PBS, counted and lysed by adding 30 µL Pierce IP lysis buffer (ThermoFisher Scientific) with HALT protease inhibitor cocktail (ThermoFisher Scientific) and rocking on ice for 5 minutes. The lysate was clarified by centrifuging at 14,000 xG for 10 minutes at 4 °C. Lysates were mixed with 4X Laemmli Sample Buffer (Bio-Rad) and heated at 95 °C for 5 minutes prior to running on a 4-15% TGX criterion gel at 150 V for 1 hour. Protein was transferred to a PVDF membrane with a Trans-Blot Turbo Transfer system (Bio-Rad) using the StandardSD (1 Amp, 25 V, 30 min) method. The membrane was blocked with 5% fat free milk in TBST for 1 hour at room temperature.

Antibodies used for western blot analysis. All primary antibodies were diluted in 5% fat free milk in TBST and incubated overnight at 4 °C with gentle rocking. We utilized antibodies directed against NCOA7 (ProteinTech, 1:1,000). NHE6 (ThermoFisher, 1:100-1:500), NHE8 (ProteinTech 1;100-1:500), NHE9 (ThermoFisher, 1:100-1:500), V-ATPase subunit E1 (ThermoFisher, 1:500), Vinculin (Millipore Sigma, 1:1,000), GFP (Abcam, 1:1,000), Nef (AIDS research and reference reagent program, 1:100-1:500), β-COP (ThermoFisher Scientific, 1:100-1:1,000), ARF-1 (ThermoFisher Scientific,1:100 -1:1000), AP-1 γ (BD Biosciences, 1:100), HA.11 (BioLegend, 1:100), FLAG-HRP (Millipore Sigma, 1:10,000-1:110,000), GAPDH (Sigma Aldrich, 1:1,000), Vif (AIDS research and reference reagent program, 1:5,000), and Vpu (AIDS research and reference reagent program 1:5,000).

Membrane staining. The following day, the blots were washed 5X with TBST with rocking for 5 minutes per wash at room temperature. All secondaries conjugated to horseradish peroxidase were diluted 1:10,000 in 5% fat free milk in TBST and incubated with the blots for 1 hour at room temperature. For detecting NCOA7, NHE6, NHE9, V-ATPase subunit E1, Nef, Vpu, β-COP, and ARF-1, blots were incubated with goat anti-rabbit IgG-HRP secondary (ThermoFisher Scientific). For detecting Vinculin, Vif, GAPDH and AP-1 γ, blots were incubated with goat anti-mouse IgG-HRP secondary (ThermoFisher Scientific or R&D Systems respectively). For detecting GFP, blots were incubated with goat anti-Chicken IgY-HRP (ThermoFisher Scientific). For detecting HA.11, rat anti-mouse IgG1 (eBioscience) was used. Blots were washed 5X with TBST for 5 minutes per wash, incubated with ECL substrate and chemiluminescent signal was visualized with a Chemidoc Imaging system (Bio-Rad).

Co-Immunoprecipitation of Proteins Bound to Nef

25 million CEM-A2 cells were transduced with ΔGPE-FLAG-Nef-IRES-NHE6, ΔGPE-FLAG-Nef-IRES or mock transduced with D10 containing no virus as described above. To inhibit excessive degradation of MHC-I and other proteins of interest by the lysosome, 48 hours post transduction, cells were collected, counted, and resuspended in R10 supplemented with 35 mM NH_4Cl at a density of 1 million cells/mL. 24 hours post NH_4Cl treatment, equal number of cells for each condition were pelleted, washed with PBS, and transferred to a pre-weighed tube. PBS was aspirated and the weight of the cell pellet was calculated. The weight of the cell pellet (in mg) was then multiplied by 10 to calculate the appropriate volume of lysis buffer (i.e. a 50 mg pellet would be lysed in 500 µL of buffer). A subset of cells was subjected to flow cytometric analysis to check that transduction rates between the viruses were similar and Nef-dependent MHC-I downmodulation occurred as expected.

Peirce IP lysis buffer (ThermoFisher Scientific) was supplemented with 1 mM phenylmethylsulfonyl fluoride (PMSF, Millipore Sigma) and 1X protease inhibitor tablet (10X solution prepared by dissolving 1 tablet in 1 mL of Pierce IP buffer, Millipore Sigma). Cell pellets were resuspended in lysis buffer according to their weight as described above and rocked on ice for 5 minutes. Lysate was clarified by centrifuging at 14,000 xG for 10 minutes at 4 °C. A fraction of lysate was saved to run as an input control. 40 µL of magnetic FLAG resin (Millipore Sigma) per 25 million cells was washed three times with 4 resin volumes of lysis buffer. Lysates were added to the resin and rotated at 4 °C for 1.5 hours. Resin was separated from the lysate with a magnetic stand, lysate was aspirated, and resin was washed 3 times with 500 µL of modified IP

buffer (Pierce IP buffer except with 0.1% NP-40 and 0.5% glycerol) with rotation at 4 °C for 5 minutes. The resin was transferred to a clean tube for the final wash.

Protein was eluted from the resin by adding a 200 ng/µL stock of 3X FLAG peptide (Millipore Sigma) diluted in modified IP buffer and agitated at room temperature for 30 minutes. Resin was separated from the eluate with a magnetic stand and eluate was collected. Eluate was concentrated from 100 µL to 30 µL by centrifuging in Amicon centrifugal filter units with a 3 kDa molecular weight cutoff (Millipore Sigma) for 1 hour at 14,000 xG at 4 °C.

4X Laemmli Sample Buffer (Bio-Rad) was mixed with all the samples and heated at 95 °C for 5 minutes. Samples were run on a 4-15% gradient acrylamide gel (Bio-Rad) at 130 V for 90 minutes. Protein was transferred to PVDF membrane at 350 mAmp for 90 minutes. The membrane was then blocked with 5% fat free milk in TBST for 1 hour at room temperature and stained as described above.

Isolation of Intact Rab11^{+} Compartments

48 hours post transduction with ΔGPE-IRES or ΔGPE-IRES-NHE6, CEM-A2 cells stably expressing FLAG-tagged Rab11 (CEM-A2-FLAG-Rab11) were pelleted (~17 million cells per sample). As a control, mock transduced CEM-A2-FLAG-Rab11 and CEM-A2 cells were included. Cells were washed 1X with KPBS (25 mM KCl, 100 mM potassium phosphate, pH 7.2) and were resuspended at a density of 1.2 million cells/mL in KPBS + HALT protease inhibitor (ThermoFisher Scientific) diluted to 1X final concentration and lysed with 50 strokes of a 2 mL Dounce homogenizer on ice. Lysate was clarified twice at 1,000 xG at 4 °C for 5 min. Aliquots of 60 µL of Anti-FLAG M2 Magnetic Beads (Millipore Sigma) were washed three times with 1 mL of lysis buffer. 20 µL of clarified lysate was saved to run as an input fraction and mixed with 10 µL of lysis buffer to produce a final volume of 30 µL. The remaining lysate was added to the beads and incubated for 50 minutes at 4 °C with rotation. Beads were separated from the lysate with a magnetic stand and unbound lysate was aspirated. Beads were washed three times with 500 µL of lysis buffer. Each wash rotated for 5 minutes at 4 °C and beads were transferred to a clean tube for the final wash. Protein was eluted from the beads by adding 30 µL of a 500 ng/µL stock of 3X FLAG peptide (Millipore Sigma) diluted in KPBS and agitated at room temperature for 45 minutes. Beads were separated from the eluate with a magnetic stand and the eluate fraction was collected. This procedure was taken and modified from dx.doi.org/10.17504/protocols.io.ewov14pjyvr2/v2. Samples were separated by SDS PAGE,

transferred using a Trans-Blot Turbo Transfer system (Bio-RAD) and analyzed via western blot as described above.

NHE6 Peptide Competition of Antibody Binding

Because western blot analysis using the NHE6 antibody (ThermoFisher Scientific) produced numerous bands, we performed a peptide competition to identify bona fide NHE6 bands. A peptide corresponding to the epitope recognized by the antibody was custom order from Biomatik (sequence of peptide: LAFGDHELVIRGTRLVLPMDDSEPPLNLLDNTRHGPA). The peptide was dissolved in a 4:1 ratio of acetonitrile:water (solvent). 5 million CEM-A2 cells were collected and lysed as described above and protein concentration was assessed using a Pierce BCA protein assay kit (ThermoFisher Scientific). 3 aliquots of 50 µg, 20 µg, or 10 µg of CEM-A2 lysate were prepared by diluting the lysate in lysis buffer in a final volume of 30 µL, separated by SDS PAGE and analyzed by western blot as described above except the membrane was blocked with 5% BSA in PBS.

3 aliquots of 10 µg of NHE6 antibody (ThermoFisher Scientific) were diluted in 5% BSA in PBS. 20 µL of solvent was added to one aliquot to produce a solvent control. 50 µg of epitope peptide describe above was added to one aliquot of antibody (5X excess the antibody amount). 100 µg of epitope peptide was added to one aliquot of antibody (10X excess the antibody amount). The antibody aliquots were pre-incubated with the peptide or solvent for 7 hours at 4 °C with rotation. After incubation with the epitope peptide or solvent, the antibodies were added to the membranes, incubated overnight at 4 °C with rocking and stained with antibody directed against NHE6 as described above.

To ensure the epitope peptide was specific to the NHE6 antibody and would not block detection of other NHEs, the experiment was performed exactly as described above, but with the NHE8 antibody (ProteinTech).

Quantification and statistical analysis

Calculation of Relative Protein Expression

For Figure 1E-I, chemiluminescent signal of the target proteins was quantified with Image Lab software (Bio-Rad) and divided by the corresponding vinculin signal to control for slight variations in total protein. The fold change of protein expression relative to GFP^- samples was calculated as follows for each target protein:

$$Protein\ Expression\ Fold\ Change = \frac{Vinculin{-}Normalized\ Protein\ Signal_{GFP+}}{Vinculin{-}Normalized\ Protein\ Signal_{GFP-}}$$

Statistical significance was determined with a One-Way ANOVA mixed effects analysis with Dunnett correction.

Quantification of Changes in Transferrin^{+} Compartment Acidity

For Figure 1J, MFIs for pHrodo and AlexFluor647 were obtained with FlowJo software for the GFP^{+} and GFP^{-} cells. The pHrodo signal was first normalized to the AlexaFluor 647 signal using the following equation to account for variations in transferrin uptake between samples:

$$Normalized\ pHrodo\ Signal = \frac{pHrodo\ MFI_{transduced}}{AlexFluor647\ MFI_{transduced}}$$

Fold change of pHrodo signal relative to the GFP^{-} cells was calculated as follows:

$$pHrodo\ Signal\ Fold\ Change = \frac{Normalized\ pHrodo\ Signal_{GFP}+}{Normalized\ pHrodo\ Signal_{GFP}-}$$

Statistical significance was determined by a paired T-test.

A similar analysis was conducted for Figure 4D and E and Figure 7C, except pHrodo signal fold change for GFP^{+} cells transduced with ΔGPE NL-GI-IRES-NHE6/8/9 and ΔGPE NL-GI-IRES or ΔGPE, GPEN, and ΔGPEF were calculated relative to mock infected cells. Statistical significance was determined by a One-Way ANOVA mixed effects analysis with Tukey correction with GraphPad Prism software.

Quantification of NHE overexpression by confocal microscopy

For Figure 3B, D, and F, cell area, integrated density, and mean grey value were obtained from Fiji software for each cell and sample of background from each image. Corrected total cell fluorescence (CTCF) was calculated as follows for each cell:

$$CTCF = Integrated\ Density_{cell} - (Area\ of\ Cell\ X\ Mean\ Fluorescence_{background})$$

CTCF for at least 30 cells transduced with the NHE overexpressing viruses or ΔGPE NL-GI-IRES were calculated. Fluorescent signal fold change for each NHE was calculated with the following equation:

$$Flourescent\ Signal\ Fold\ Change = \frac{CTCF_{NHE-overepxressing\ cell\ or\ \Delta GPE-IRES\ cell}}{Mean\ CTCF_{\Delta GPE-IRES}}$$

The resulting values were plotted as bar graphs and statistical significance was determined by an unpaired T-test with GraphPad Prism software.

Pearson's correlation coefficients displayed in Figure 3H, J, and L were obtained with Nikon Elements Advanced Research (AR) software.

Calculation of Fold Change of Nef-dependent MHC-I and CD4 downmodulation between ΔGPE-IRES-NHE6/8/9, ΔGPE-IRES, and ΔGPEN or ΔGPE, ΔGPEN, and ΔGPEF

As shown in Figure 5B (top panel), downmodulation of MHC-I by Nef, referred to as Nef activity, was calculated by performing flow cytometric analysis of its expression. Median fluorescent intensities (MFIs) for MHC-I expression of live GFP^- cells (untransduced) and GFP^+ cells (transduced) was calculated with FlowJo data analysis software. These values were applied to the following equation:

$$MHC-I\ Downmodulation\ or\ Nef\ Activity = \frac{MFI_{untransduced}}{MFI_{transduced}}$$

For Figures 4B, to determine if MHC-I downmodulation was impacted by NHE overexpression, its downmodulation was calculated as described above for primary $CD4^+$ T cells transduced with ΔGPE-IRES-NHE6/8/9, ΔGPE-IRES, or ΔGPEN. The fold change in downmodulation of MHC-I for each virus compared to ΔGPE NL-GI-IRES was calculated as follows:

$$MHC-I\ Downmodulation\ Fold\ Change = \frac{MHC-I\ Downmodulation_{\Delta GPE-IRES-NHE\ or\ \Delta GPEN}}{MHC-I\ Downmodulation_{\Delta GPE-IRES}}$$

CD4 downmodulation was calculated as described for MHC-I, except that CD4 median fluorescence intensity (MFI) was utilized. For figure 4C, CD4 downmodulation fold change was calculated exactly as described for MHC-I. Statistical significance for Figure 4B and C was determined with a One-Way ANOVA mixed effects analysis with Dunnett correction. For Figure 5B, statistical significance between downmodulation of MHC-I and CD4 for ΔGPE-IRES and ΔGPE-FLAG-Nef-IRES was determined with paired T test calculated with GraphPad Prism software.

As shown in Figure 7D, MHC-I downmodulation fold change for ΔGPE, ΔGPEN, and ΔGPEF relative to ΔGPE was calculated with the equation above with ΔGPE MHC-I downmodulation in the denominator. Statistical significance was determined with a One-Way ANOVA mixes effects analysis with Dunnett correction.

Quantification of Lysosome neutralization in response to NHE overexpression

For Figure 4F, the extent of lysosome acidification in response to NHE overexpression was evaluated by obtaining Lysotracker MFIs for GFP$^+$ cells transduced with ΔGPE NL-GI-IRES-NHE6/8/9, ΔGPE NL-GI-IRES, or ΔGPEN from FlowJo software. Fold change of Lysotracker signal in response to NHE overexpression or ΔGPEN compared to no overexpression was calculated with the following equation:

$$Lysotracker\ MFI\ Fold\ Change = \frac{Lysotracker\ MFI_{\Delta GPE-IRES-NHE}}{Lysotracker\ MFI_{\Delta GPE-IRES}}$$

Statistical significance for Figure 4F was determined with a one-way ANOVA mixed effects analysis with Dunnett correction performed with GraphPad Prism software.

Calculation of CMA and Baf A1 Dose response curves and IC_{50} values for Nef Activity, Transferrin$^+$ Compartment Neutralization, and Lysotracker

At every concentration of CMA or Baf A1 and solvent tested, MHC-I downmodulation was calculated as described above. MHC-I downmodulation in the presence of CMA or Baf A1 was compared to solvent using the following equation for each concentration of CMA or Baf A1 tested:

$$Sovlent\ Normalized\ Nef\ Activity\ = \frac{MHC-I\ Downmodulation_{CMA\ or\ Baf\ A1\ treated\ sample}}{MHC-I\ Downmodulation_{solvent\ treated\ sample}}$$

The resulting data were plotted to produce dose-response curves seen in Figure 2A, B, D, and E. The amount of CMA or Baf A1 required to inhibit 50% of Nef activity (CMA IC_{50} or Baf A1 $IC_{50,}$ Nef Activity), as seen in Figure 2C and F, were calculated with GraphPad Prism software.

The impact of CMA or Baf A1 on lysosome acidification was calculated exactly like that for Nef Activity, except using Lysotracker MFIs for GFP$^-$ cells instead of MHC-I downmodulation in the numerator and denominator (Figure 2A and Figure 2D).

Transferrin$^+$ compartmental neutralization by CMA or Baf A1 was assessed by flow cytometric analysis. The pHrodo signal was normalized to the AF-647 signal using the normalized pHrodo signal equation above. At every concentration of CMA, Baf A1, or solvent tested, the normalized pHrodo signal of the GFP$^+$ CMA or Baf A1 treated cells was compared to the solvent treated cells using the following equation:

$$Sovlent\ Normalized\ pHrodo\ Signal = \frac{Normalized\ pHrodo\ Signal_{CMA\ or\ Baf\ A1\ treated\ sample}}{Normalized\ pHrodo\ Signal_{solvent\ treated\ sample}}$$

The resulting data points were plotted to produce the dose-response curve shown in Figure 2B and 2E. The amount of CMA or Baf A1 required to reduce the pHrodo signal by 50% (CMA or Baf A1 IC_{50}, pHrodo-Transferrin MFI) was obtained from GraphPad Prism software. Further, the IC_{50}s for Nef activity, pHrodo-transferrin MFI, and Lysotracker MFI were compared as shown in Figure 2C and 2F. Statistical significance was determined with a One-Way ANOVA mixed effects analysis with Dunnet correction calculated with GraphPad Prism software.

Quantification of protein complex formation by Nef during NHE6 overexpression

Western blots of co-immunoprecipitation experiments of CEM-A2 lysates transduced with ΔGPE-FLAG-Nef-IRES, ΔGPE-FLAG-Nef-IRES-NHE6, or mock transduced were imaged on an iBright Imaging System (ThermoFisher Scientific). Intensity of protein bands was obtained with ImageStudio software (LI-COR). To account for slight variations in the amount of Nef pulled down between samples, chemiluminescent signals of the target proteins were first normalized to Nef intensities using the following equation:

$$Nef\ Normalized\ Target\ Protein\ Signal = \frac{Target\ Protein\ Signal}{Nef\ Signal}$$

The fold change of protein bound to Nef between ΔGPE-FLAG-Nef-IRES and ΔGPE-FLAG-Nef-IRES-NHE6 was then calculated as follows:

$$Fold\ Change\ of\ Protein\ Bound\ to\ Nef = \frac{Nef\ Normalized\ Target\ Protein\ Signal_{\Delta GPE-FLAG-Nef-IRES-NHE6}}{Nef\ Normalized\ Target\ Protein\ Signal_{\Delta GPE-FLAG-Nef-IRES}}$$

This was graphed as shown in Figure 5E. Statistically significant changes binding of each target protein to Nef were evaluated with a paired T test using GraphPad Prism software.

Quantification of Nef Present in $Rab11^+$ Compartments with and without NHE6 Overexpression

Western blots of the contents of precipitated intact $Rab11^+$ compartments were imaged on a Chemidoc Imaging system (Bio-Rad). Intensity of protein bands was obtained with Image Lab software (Bio-Rad). To account for slight variations in the amount of Rab11 pulled down between samples, Nef signal was first normalized to the corresponding Rab11 signal with the following equation:

$$Rab11\ Normalized\ Nef\ Signal = \frac{Nef\ Signal}{Rab11\ Signal}$$

The fold change of the amount of Nef found in isolated $Rab11^+$ compartments relative to transduction with ΔGPE-NL-GI-IRES was calculated as follows:

$$Fold\ Change\ Nef\ in\ Rab11 + Compartments = \frac{Rab11\ Normalized\ Nef\ Signal_{\Delta GPE-NHE6}}{Rab11\ Normalized\ Nef\ Signal_{\Delta GPE-IRES}}$$

The resulting values were graphed as shown in Figure 6E. Statistical significance was determined with a Paired T Test calculated with GraphPad Prism software.

REFERENCES

1. Caffrey, M., and Lavie, A. (2021). pH-Dependent Mechanisms of Influenza Infection Mediated by Hemagglutinin. Front Mol Biosci *8*, 777095. https://doi.org/10.3389/fmolb.2021.777095.

2. Doyle, T., Moncorgé, O., Bonaventure, B., Pollpeter, D., Lussignol, M., Tauziet, M., Apolonia, L., Catanese, M.-T., Goujon, C., and Malim, M.H. (2018). The interferon-inducible isoform of NCOA7 inhibits endosome-mediated viral entry. Nat Microbiol *3*, 1369–1376. https://doi.org/10.1038/s41564-018-0273-9.

3. Khan, H., Winstone, H., Jimenez-Guardeño, J.M., Graham, C., Doores, K.J., Goujon, C., Matthews, D.A., Davidson, A.D., Rihn, S.J., Palmarini, M., et al. (2021). TMPRSS2 promotes SARS-CoV-2 evasion from NCOA7-mediated restriction. PLOS Pathogens *17*, e1009820. https://doi.org/10.1371/journal.ppat.1009820.

4. Miyauchi, K., Kim, Y., Latinovic, O., Morozov, V., and Melikyan, G.B. (2009). HIV Enters Cells via Endocytosis and Dynamin-Dependent Fusion with Endosomes. Cell *137*, 433–444. https://doi.org/10.1016/j.cell.2009.02.046.

5. Nakamura, N., Tanaka, S., Teko, Y., Mitsui, K., and Kanazawa, H. (2005). Four Na+/H+ Exchanger Isoforms Are Distributed to Golgi and Post-Golgi Compartments and Are Involved in Organelle pH Regulation*. Journal of Biological Chemistry *280*, 1561–1572. https://doi.org/10.1074/jbc.M410041200.

6. Ohgaki, R., Matsushita, M., Kanazawa, H., Ogihara, S., Hoekstra, D., and van IJzendoorn, S.C.D. (2010). The Na+/H+ Exchanger NHE6 in the Endosomal Recycling System Is Involved in the Development of Apical Bile Canalicular Surface Domains in HepG2 Cells. Mol Biol Cell *21*, 1293–1304. https://doi.org/10.1091/mbc.E09-09-0767.

7. Xinhan, L., Matsushita, M., Numaza, M., Taguchi, A., Mitsui, K., and Kanazawa, H. (2011). Na+/H+ exchanger isoform 6 (NHE6/SLC9A6) is involved in clathrin-dependent endocytosis of transferrin. Am J Physiol Cell Physiol *301*, C1431-1444. https://doi.org/10.1152/ajpcell.00154.2011.

8. Painter, M.M., Zimmerman, G.E., Merlino, M.S., Robertson, A.W., Terry, V.H., Ren, X., McLeod, M.R., Gomez-Rodriguez, L., Garcia, K.A., Leonard, J.A., et al. (2020). Concanamycin A counteracts HIV-1 Nef to enhance immune clearance of infected primary cells by cytotoxic T lymphocytes. Proceedings of the National Academy of Sciences *117*, 23835–23846. https://doi.org/10.1073/pnas.2008615117.

9. Roeth, J.F., Williams, M., Kasper, M.R., Filzen, T.M., and Collins, K.L. (2004). HIV-1 Nef disrupts MHC-I trafficking by recruiting AP-1 to the MHC-I cytoplasmic tail. J Cell Biol *167*, 903–913. https://doi.org/10.1083/jcb.200407031.

10. Kasper, M.R., and Collins, K.L. (2003). Nef-Mediated Disruption of HLA-A2 Transport to the Cell Surface in T Cells. Journal of Virology *77*, 3041–3049. https://doi.org/10.1128/jvi.77.5.3041-3049.2003.

11. Schaefer, M.R., Wonderlich, E.R., Roeth, J.F., Leonard, J.A., and Collins, K.L. (2008). HIV-1 Nef Targets MHC-I and CD4 for Degradation Via a Final Common β-COP–Dependent Pathway in T Cells. PLOS Pathogens *4*, e1000131. https://doi.org/10.1371/journal.ppat.1000131.

12. Doyle, T., Moncorgé, O., Bonaventure, B., Pollpeter, D., Lussignol, M., Tauziet, M., Apolonia, L., Catanese, M.-T., Goujon, C., and Malim, M.H. (2019). Author Correction: The interferon-inducible isoform of NCOA7 inhibits endosome-mediated viral entry. Nat Microbiol *4*, 539. https://doi.org/10.1038/s41564-019-0366-0.

13. Brett, C.L., Wei, Y., Donowitz, M., and Rao, R. (2002). Human Na+/H+ exchanger isoform 6 is found in recycling endosomes of cells, not in mitochondria. American Journal of Physiology-Cell Physiology *282*, C1031–C1041. https://doi.org/10.1152/ajpcell.00420.2001.

14. Ilie, A., Boucher, A., Park, J., Berghuis, A.M., McKinney, R.A., and Orlowski, J. (2020). Assorted dysfunctions of endosomal alkali cation/proton exchanger SLC9A6 variants linked to Christianson syndrome. J Biol Chem *295*, 7075–7095. https://doi.org/10.1074/jbc.RA120.012614.

15. Ilie, A., Gao, A.Y.L., Reid, J., Boucher, A., McEwan, C., Barrière, H., Lukacs, G.L., McKinney, R.A., and Orlowski, J. (2016). A Christianson syndrome-linked deletion mutation (Δ287ES288) in SLC9A6 disrupts recycling endosomal function and elicits neurodegeneration and cell death. Mol Neurodegener *11*, 63. https://doi.org/10.1186/s13024-016-0129-9.

16. Ilie, A., Weinstein, E., Boucher, A., McKinney, R.A., and Orlowski, J. (2014). Impaired posttranslational processing and trafficking of an endosomal Na+/H+ exchanger NHE6 mutant (Δ370WST372) associated with X-linked intellectual disability and autism. Neurochemistry International *73*, 192–203. https://doi.org/10.1016/j.neuint.2013.09.020.

17. Pruett, B.S., Pinner, A.L., Kim, P., and Meador-Woodruff, J.H. (2023). Altered distribution and localization of organellar Na+/H+ exchangers in postmortem schizophrenia dorsolateral prefrontal cortex. Transl Psychiatry *13*, 1–10. https://doi.org/10.1038/s41398-023-02336-2.

18. Mayle, K.M., Le, A.M., and Kamei, D.T. (2012). The Intracellular Trafficking Pathway of Transferrin. Biochim Biophys Acta *1820*, 264–281. https://doi.org/10.1016/j.bbagen.2011.09.009.

19. Wonderlich, E.R., Leonard, J.A., Kulpa, D.A., Leopold, K.E., Norman, J.M., and Collins, K.L. (2011). ADP Ribosylation Factor 1 Activity Is Required To Recruit AP-1 to the Major Histocompatibility Complex Class I (MHC-I) Cytoplasmic Tail and Disrupt MHC-I Trafficking in HIV-1-Infected Primary T Cells. Journal of Virology *85*, 12216–12226. https://doi.org/10.1128/jvi.00056-11.

20. Park, H., Hundley, F.V., Yu, Q., Overmyer, K.A., Brademan, D.R., Serrano, L., Paulo, J.A., Paoli, J.C., Swarup, S., Coon, J.J., et al. (2022). Spatial snapshots of amyloid precursor protein intramembrane processing via early endosome proteomics. Nat Commun *13*, 6112. https://doi.org/10.1038/s41467-022-33881-x.

21. Cotter, K., Stransky, L., McGuire, C., and Forgac, M. (2015). Recent Insights into the Structure, Regulation, and Function of the V-ATPases. Trends Biochem Sci *40*, 611–622. https://doi.org/10.1016/j.tibs.2015.08.005.

22. Trombetta, E.S., Ebersold, M., Garrett, W., Pypaert, M., and Mellman, I. (2003). Activation of Lysosomal Function During Dendritic Cell Maturation. Science *299*, 1400–1403. https://doi.org/10.1126/science.1080106.

23. Kasper, M.R., and Collins, K.L. (2003). Nef-Mediated Disruption of HLA-A2 Transport to the Cell Surface in T Cells. Journal of Virology *77*, 3041–3049. https://doi.org/10.1128/jvi.77.5.3041-3049.2003.

24. Schaefer, M.R., Wonderlich, E.R., Roeth, J.F., Leonard, J.A., and Collins, K.L. (2008). HIV-1 Nef Targets MHC-I and CD4 for Degradation Via a Final Common β-COP–Dependent Pathway in T Cells. PLOS Pathogens *4*, e1000131. https://doi.org/10.1371/journal.ppat.1000131.

25. Wonderlich, E.R., Leonard, J.A., Kulpa, D.A., Leopold, K.E., Norman, J.M., and Collins, K.L. (2011). ADP Ribosylation Factor 1 Activity Is Required To Recruit AP-1 to the Major Histocompatibility Complex Class I (MHC-I) Cytoplasmic Tail and Disrupt MHC-I Trafficking in HIV-1-Infected Primary T Cells. Journal of Virology *85*, 12216–12226. https://doi.org/10.1128/jvi.00056-11.

26. Painter, M.M., Zimmerman, G.E., Merlino, M.S., Robertson, A.W., Terry, V.H., Ren, X., McLeod, M.R., Gomez-Rodriguez, L., Garcia, K.A., Leonard, J.A., et al. (2020). Concanamycin A counteracts HIV-1 Nef to enhance immune clearance of infected primary cells by cytotoxic T lymphocytes. Proceedings of the National Academy of Sciences *117*, 23835–23846. https://doi.org/10.1073/pnas.2008615117.

27. Roeth, J.F., Williams, M., Kasper, M.R., Filzen, T.M., and Collins, K.L. (2004). HIV-1 Nef disrupts MHC-I trafficking by recruiting AP-1 to the MHC-I cytoplasmic tail. J Cell Biol *167*, 903–913. https://doi.org/10.1083/jcb.200407031.

28. Bergeron, J.R.C., Huthoff, H., Veselkov, D.A., Beavil, R.L., Simpson, P.J., Matthews, S.J., Malim, M.H., and Sanderson, M.R. (2010). The SOCS-box of HIV-1 Vif interacts with ElonginBC by induced-folding to recruit its Cul5-containing ubiquitin ligase complex. PLoS Pathog *6*, e1000925. https://doi.org/10.1371/journal.ppat.1000925.

29. Sharkey, M., Sharova, N., Mohammed, I., Huff, S.E., Kummetha, I.R., Singh, G., Rana, T.M., and Stevenson, M. (2019). HIV-1 Escape from Small-Molecule Antagonism of Vif. mBio *10*, 10.1128/mbio.00144-19. https://doi.org/10.1128/mbio.00144-19.

30. Stanley, B.J., Ehrlich, E.S., Short, L., Yu, Y., Xiao, Z., Yu, X.-F., and Xiong, Y. (2008). Structural insight into the human immunodeficiency virus Vif SOCS box and its role in human E3 ubiquitin ligase assembly. J Virol *82*, 8656–8663. https://doi.org/10.1128/JVI.00767-08.

31. Kuo, R.-L., Lin, Y.-H., Wang, R.Y.-L., Hsu, C.-W., Chiu, Y.-T., Huang, H.-I., Kao, L.-T., Yu, J.-S., Shih, S.-R., and Wu, C.-C. (2015). Proteomics Analysis of EV71-Infected Cells Reveals the Involvement of Host Protein NEDD4L in EV71 Replication. J. Proteome Res. *14*, 1818–1830. https://doi.org/10.1021/pr501199h.

32. Fraisier, C., Koraka, P., Belghazi, M., Bakli, M., Granjeaud, S., Pophillat, M., Lim, S.M., Osterhaus, A., Martina, B., Camoin, L., et al. (2014). Kinetic Analysis of Mouse Brain Proteome Alterations Following Chikungunya Virus Infection before and after Appearance of Clinical Symptoms. PLOS ONE *9*, e91397. https://doi.org/10.1371/journal.pone.0091397.

33. Baik, S.Y., Yun, H.S., Lee, H.J., Lee, M.H., Jung, S.E., Kim, J.W., Jeon, J.P., Shin, Y.K., Rhee, H.S., Kimm, K.C., et al. (2007). Identification of stathmin 1 expression induced by Epstein–Barr virus in human B lymphocytes. Cell Prolif *40*, 268–281. https://doi.org/10.1111/j.1365-2184.2007.00429.x.

34. Muramoto, Y., Shoemaker, J.E., Le, M.Q., Itoh, Y., Tamura, D., Sakai-Tagawa, Y., Imai, H., Uraki, R., Takano, R., Kawakami, E., et al. (2014). Disease Severity Is Associated with Differential Gene Expression at the Early and Late Phases of Infection in Nonhuman Primates Infected with Different H5N1 Highly Pathogenic Avian Influenza Viruses. J Virol *88*, 8981–8997. https://doi.org/10.1128/JVI.00907-14.

35. Prasad, H. (2021). Protons to Patients: targeting endosomal Na+ /H+ exchangers against COVID-19 and other viral diseases. FEBS J *288*, 5071–5088. https://doi.org/10.1111/febs.16163.

36. Slonchak, A., Clarke, B., Mackenzie, J., Amarilla, A.A., Setoh, Y.X., and Khromykh, A.A. (2019). West Nile virus infection and interferon alpha treatment alter the spectrum and the levels of coding and noncoding host RNAs secreted in extracellular vesicles. BMC Genomics *20*, 474. https://doi.org/10.1186/s12864-019-5835-6.

37. Lu, X., Yu, H., Liu, S.H., Brodsky, F.M., and Peterlin, B.M. (1998). Interactions between HIV1 Nef and vacuolar ATPase facilitate the internalization of CD4. Immunity *8*, 647–656. https://doi.org/10.1016/s1074-7613(00)80569-5.